Alma Mater Studiorum · Università di Bologna

Scuola di Scienze
Corso di Laurea Magistrale in Fisica del Sistema Terra

Validation of an intermediate-complexity flood risk model for climate change adaptation

Relatore:
Prof. Silvana Di Sabatino

Correlatore:
Dott. Paolo Ruggieri

Presentata da:
Vincenzo Senigalliesi

Anno Accademico 2021/2022

Contents

List of Figures

List of Tables

Listings

Abstract

In questo lavoro di tesi viene presentato e validato un modello di rischio di alluvione a complessità intermedia per scenari climatici futuri. Questo modello appartiene a quella categoria di strumenti che mirano a soddisfare le esigenze identificate dal World Climate Research Program (WRCP) per affrontare gli effetti del cambiamento climatico. L'obiettivo perseguito è quello di sviluppare, seguendo un approccio "bottom-up" al rischio climatico regionale, strumenti che possano aiutare i decisori a realizzare l'adattamento ai cambiamenti climatici. Il modello qui presentato è interamente basato su dati open-source forniti dai servizi Copernicus. Il contributo di questo lavoro di tesi riguarda lo sviluppo di un modello, formulato da [1](Ruggieri et al.), per stimare i danni di eventi alluvionali fluviali per specifici livelli di riscaldamento globale (GWL). Il modello è stato testato su tre bacini idrografici di medie dimensioni in Emilia-Romagna, Panaro, Reno e Secchia. In questo lavoro, il modello viene sottoposto a test di sensibilità rispetto a un'ipotesi enunciata nella formulazione del modello, poi vengono effettuate analisi relative all'ensemble multi-modello utilizzato per le proiezioni. Il modello viene quindi validato, confrontando i danni stimati nel clima attuale per i tre fiumi con i danni osservati e confrontando le portate simulate con quelle osservate. Infine, vengono stimati i danni associati agli eventi alluvionali in tre scenari climatici futuri caratterizzati da GWL di 1.5°C, 2.0°C e 3.0°C.

Chapter 1

Introduction

The climate is often defined as the "average weather, or more rigorously, as the statistical description in terms of the mean and variability of relevant quantities over a period of time ranging from months to thousands or millions of year" [2](R. Shukla et al.). Consequently, when we deal with climate change, we are treated with deviations, which persist for long periods, of mean and variability from the ones defined by the climate. The so-called "radiative balance" is a mechanism that determines the state of the climate, if the balance is satisfied we will say that the state is in a certain configuration. One of the mechanisms which lead the climate to change is called climate forcing. Such forcing can be considered perturbations of a stable configuration; the earth system, in response, through the radiative balance reaches a new stable configuration. A climate forcing can be natural based, an example of natural forcing can be represented by changes in orbital parameters or in solar activity that can lead to reaching a new colder or warmer configuration, creating the so-called glacial and interglacial periods. The unequivocal knowledge of such phenomenon allowed us to identify a forcing different from the natural, the anthropic one. Such forcing is typically represented by the greenhouse gas emission, that drives the earth system towards a new stable configuration, to satisfy the radiative balance, warmer with respect to pre-industrial conditions (1861-1890). "The Intergovernmental Panel on Climate Change (IPCC) is an intergovernmental body of the United Nations responsible for advancing knowledge on human-induced climate change which provide periodic reports concerning the state of the climate" [3]. The IPCC Assessment Report 5 (2014) identified four possible Representative Concentration Pathways (RCPs) scenarios, as radiative forcing that came from 2.6, 4.5, 6.0 to 8.5 Wm^{-2}, that can be reached at the year 2100. The AR6 (2021) introduces new scenarios based on the Shared Socio-Economic Pathways (SSPs), which take into account the fact that radiative forcing levels can be reached by different pathways of CO_2, non CO_2 greenhouse gases (GHGs), aerosols and land use [4](IPCC AR6 WG1). According to [3](IPCC AR6 WG1) global warming variations are linked quasi-linearly to CO_2 emission, while regionally changes, including extreme events, scale quasi-linearly with changes in global warming, independently by emissions scenarios. In addition, even if some regional changes scale robustly with surface temperature increase, the effects on the local scale can be different. For example, " emissions scenarios with the same radiative forcing can have different regional extreme precipitation responses resulting from different aerosol forcing" [3]. Therefore the realization of a generic emission pathway is characterized by uncertainties that consequently, will involve uncertainties in variables projections. A different point o view to represent the information concerning the future climate could be to consider certain Global Warming Levels (GWLs) e see what happens, to the impact, if a GWL is reached rather than another; this approach is represented qualitatively in Fig. 1.1. Therefore, given a general forcing, these induce a global mean response which has a physical and

social/economic impact on a local scale through a regional climate response. Assess future changes in extreme events impacts as a function of GWL, allows us to separate the uncertainty resulting from global warming in response to emission scenarios, and the one due to regional climate response resulting from certain GWLs. Therefore, if the aim is to make projections on a regional scale at certain GWLs, the ones based on time ranges and emissions scenarios have too much uncertainty caused by differences in model global transient climate response (shaded grey area in Fig. 1.1). Instead, by partitioning the uncertainty, i.e. without taking into account the forcing which determines a certain GWL but GWL itself, we can recognize the uncertainty of physical and social/economic impact associated with such GWL.

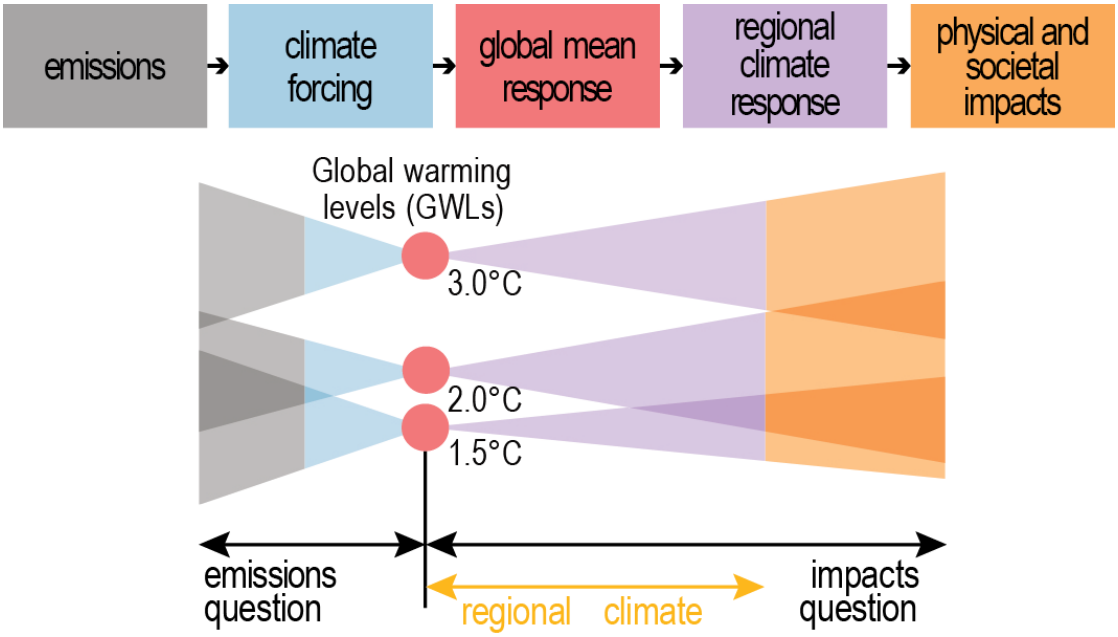

Figure 1.1: Schematic representation of the relationship between emissions scenarios, global warming levels (GWLs), regional climate responses, and impacts. Image taken from [3].

Since the early studies on climate change, the focus of research has been oriented to improve the quality of the climate data which describes the past and actual state of the earth system to make better projections of the future [5](Rogrigues et al.). The scientific community then realized that its purpose, in addition to improving the data quality, should also be to understand how to face the consequences of climate change. The two approaches actionable to deal with the consequences of climate change are "mitigation" and "adaptation", which respectively aim to, reduce climate change and adapt life in a changing climate context. The challenges that climate science faces nowadays requires tools that can be used by a range of potential users to quantify how climate risks are affected by climate change and the associated uncertainty. In such context, the World Climate Research Program (WRCP) defined the lighthouse activities of My Climate Risk with a special focus on the local scale. Two possible approaches can be followed in order to address climate change, both of them are represented in Fig. 1.2. The "top-down" approach, through mitigation measures, provides a way, for government policies on a global scale, to respect the Paris agreement target of 1.5°C. The problem which affect such approach concerns the fact that all the policy measures which arise from it, are a sort of action on a large scale, which means that its effects are weakly perceived by the local communities. Moreover, as pointed out by [5](Rodreigues

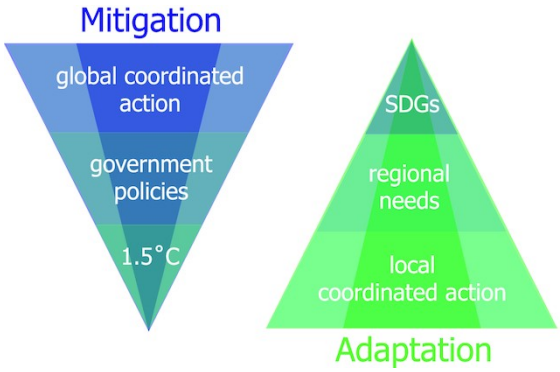

Figure 1.2: Contrast between the "top-down" approach in climate-change science, which is needed for mitigation action, and the "bottom-up" approach needed for adaptation action. Image taken from [5].

et al.) traditional approaches to adaptation, which were performed by using mitigation tools, were ineffective. In that sense, a "bottom-up" approach, which pursues adaptation rather than mitigation, is actionable in order to give to policymakers, on sub-regional and local scale, tools different from the mitigation ones to deal with climate change. Is on that approach on which My Risk is based, that is "developing a new framework for assessing and explaining regional climate risk using all the available sources of climate information and by making it meaningful at the local scale" [6].

Since the saturation vapour pressure increases with temperature, the higher the atmosphere temperature, the greater will be the water-holding capacity, which could increase extreme precipitation [7](Dankers et al.). On a local scale, other effects due to climate change must be taken into account. Although a warm Earth can release more latent heat that can invigorate storms, the changing in atmosphere aerosol composition can affect the efficiency of converting moisture into precipitation, resulting in a change in the characteristics of extreme precipitation events [3]. The are a lot of sources of uncertainty regarding future extreme precipitation events, depending on projections about, dynamics, aerosol concentrations, the pattern of surface temperature, changes in atmospheric and ocean circulation, etc. As well as there is uncertainty in the impact of such events depending, especially, on changes in land use. Therefore the effects due to some thermodynamic process are assessed with high confidence, while dynamic aspects of future climate are affected by low confidence, mainly on a local scale. As shown by Fig. 1.3, and according to [3], the annual maximum daily precipitation (Rx1day) has increased during the mid-20th century over land, "the percentage of observing stations with statistically significant increases in annual maximum daily precipitation (Rx1day) is larger than expected by chance" [3]. What is found is an intensification of light, moderate, heavy daily and sub-daily precipitation, although the last one remains low confidence at a global scale. An increase in extreme sub-daily precipitation is found in Italy from [8](Libertino et al.), which also highlights the necessity to use a small scale to perform an efficient local analysis. This type of precipitation, in Italy, are the ones that causes flooding events. In this regard, as shown by Fig. 1.3, in Europe during the 1950–2018 periods, the number of regions in which an increase in Rx1day is observed is larger than the ones in which it decreased.

Following [3], a flood event is an inundation of land. In this work, we will refer only to river floods. A such event happens when the banks of the rivers are not able anymore to harness the streamflow. "The AR5, assessed with low confidence for observed changes in the magnitudes or frequency of floods at the global scale" [3], but further papers found an increase of frequency and magnitude in some regions and a decrease in some others.

Since most of the successive papers are focused on a local scale analysis, it is difficult to assess the global and regional scale. Moreover, the measurements of streamflow rivers are not homogeneously distributed with some spatial gap, which lead the assessment of observed trends more difficult. The principal drivers for flood events in Europe are the extreme precipitation events in the western and the snowmelting in the eastern. There are regions in which both mechanisms are present, and this cause to extreme river flooding over large areas. Even if on a global scale the confidence about observed trends in the magnitude an frequency of floods is low, if regional scales are considered some high confidence assessments can be performed.

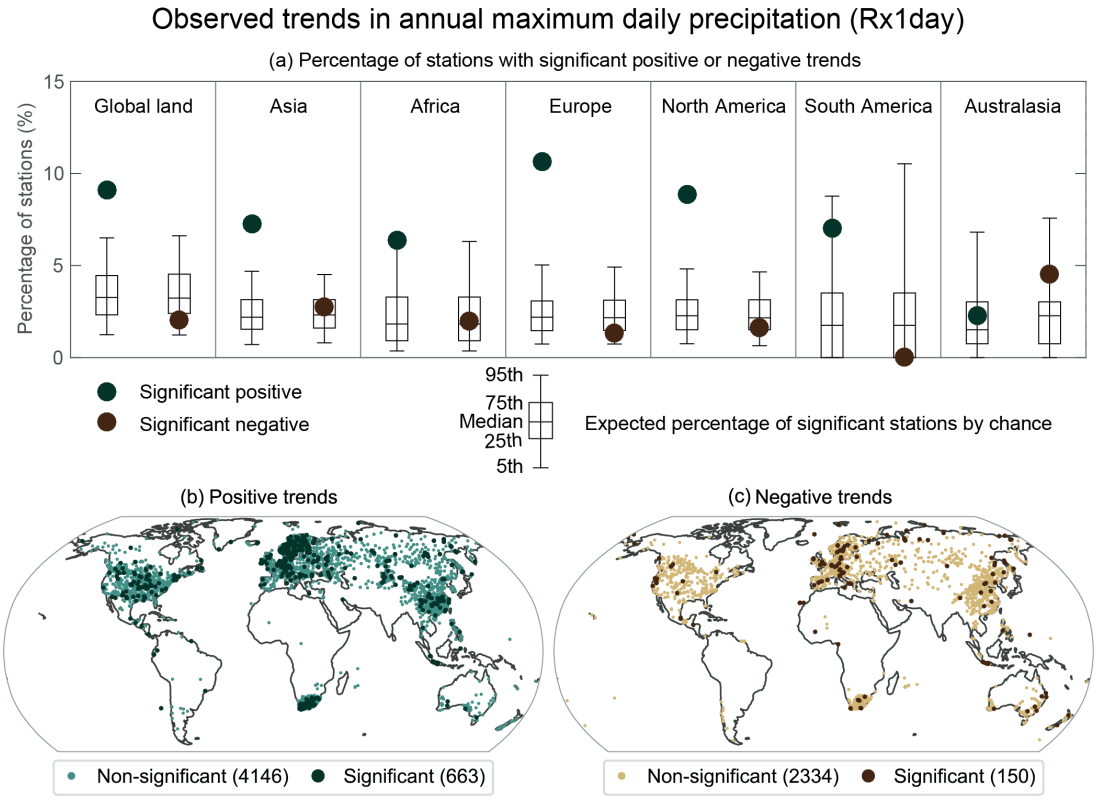

Figure 1.3: Signs and significance of the observed trends in annual maximum daily precipitation (Rx1day) during 1950–2018 at 8345 stations with sufficient data. (a) Percentage of stations with statistically significant trends in Rx1day; green dots show positive trends and brown dots negative trends. Box and 'whisker' plots indicate the expected percentage of stations with significant trends due to chance estimated from 1000 bootstrap realizations under a no-trend null hypothesis. The boxes mark the median, 25th percentile, and 75th percentile. The upper and lower whiskers show the 97.5th and the 2.5th percentiles, respectively. Maps of stations with positive (b) and negative (c) trends. The light colour indicates stations with non-significant trends, and the dark colour stations with significant trends. Image taken from [3].

In the Mediterranean area, a decreasing of flood events trend is observed even if for Rx1day, one of the mechanisms from which floods events depend, a increases trend is observed. According to [3], "the seasonality of floods is changed in cold regions where the snowmelt dominates with high confidence", while there is low confidence about a decrease in floods in the Mediterranean regions.

For heavy precipitation, according to [4] it is very likely that extreme events will be more frequent, moreover it is found that, the rate of increase in Rx1day with warming

does not depend on the forcing scenario. Fig. 1.4 shows the relative changes, in terms of intensity, of Rx1day as a function of return periods of 10 and 50 years for precipitation over land with respect to the 1850–1900 baseline under four different degree scenarios. Therefore, with high confidence, the extreme precipitation as a function of return periods, respectively equal to 10 and 50 years events, increases in magnitude, as the temperature increase.

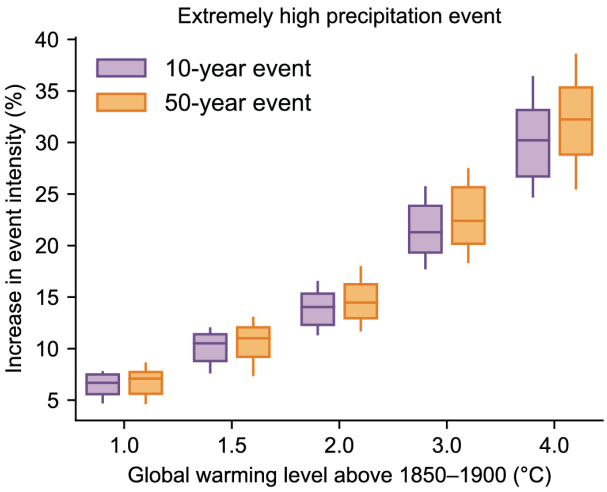

Figure 1.4: Projected changes in the intensity of extreme precipitation events under 1°C, 1.5°C, 2°C, 3°C, and 4°C global warming levels relative to the 1850–1900 baseline. Extreme precipitation events are defined as the Rx1day that was exceeded on average once during a 10-year period (10-year event, blue) and once during a 50-year period (50-year event, orange) during the 1850–1900 base period. Results are shown for the global land. Image taken from [3].

Following [3], Fig. 1.5 represents the spatial patterns of Rx1day changes for different degree scenarios, by showing an increase of confidence extension as the temperature of the scenario increase. The different changes in different regions are due to internal variability. Extreme precipitation events increase in the larger part of the globe, except for Southern Europe around the Mediterranean basin for low warming levels.

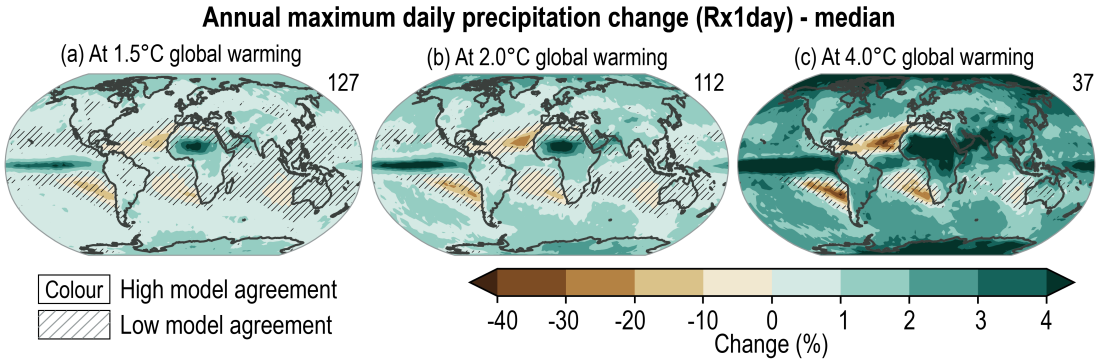

Figure 1.5: Projected changes in annual maximum daily precipitation at (a) 1.5°C, (b) 2°C, and (c) 4°C of global warming compared to the 1850–1900 baseline. Results are based on simulations from the Coupled Model Intercomparison Project Phase 6 (CMIP6) multi-model ensemble under the Shared Socio-economic Pathway (SSP), SSP1-1.9, SSP1-2.6, SSP2-4.5, SSP3-7.0, and SSP5-8.5 scenarios. The numbers on the top right indicate the number of simulations included. Uncertainty is represented using the simple approach: no overlay indicates regions with high model agreement, where $\geq 80\%$ of models agree on the sign of change; diagonal lines indicate regions with low model agreement, where $< 80\%$ of models agree on the sign of change. Image taken from [3].

The two panels in Fig. 1.6 shown the spatial pattern in the Mediterranean region to focus attention on Italy. In that region the climate signal gradually emerges, by increasing the temperature of warming level, by highlighting positive changes compared to the 1950-1900 baseline.

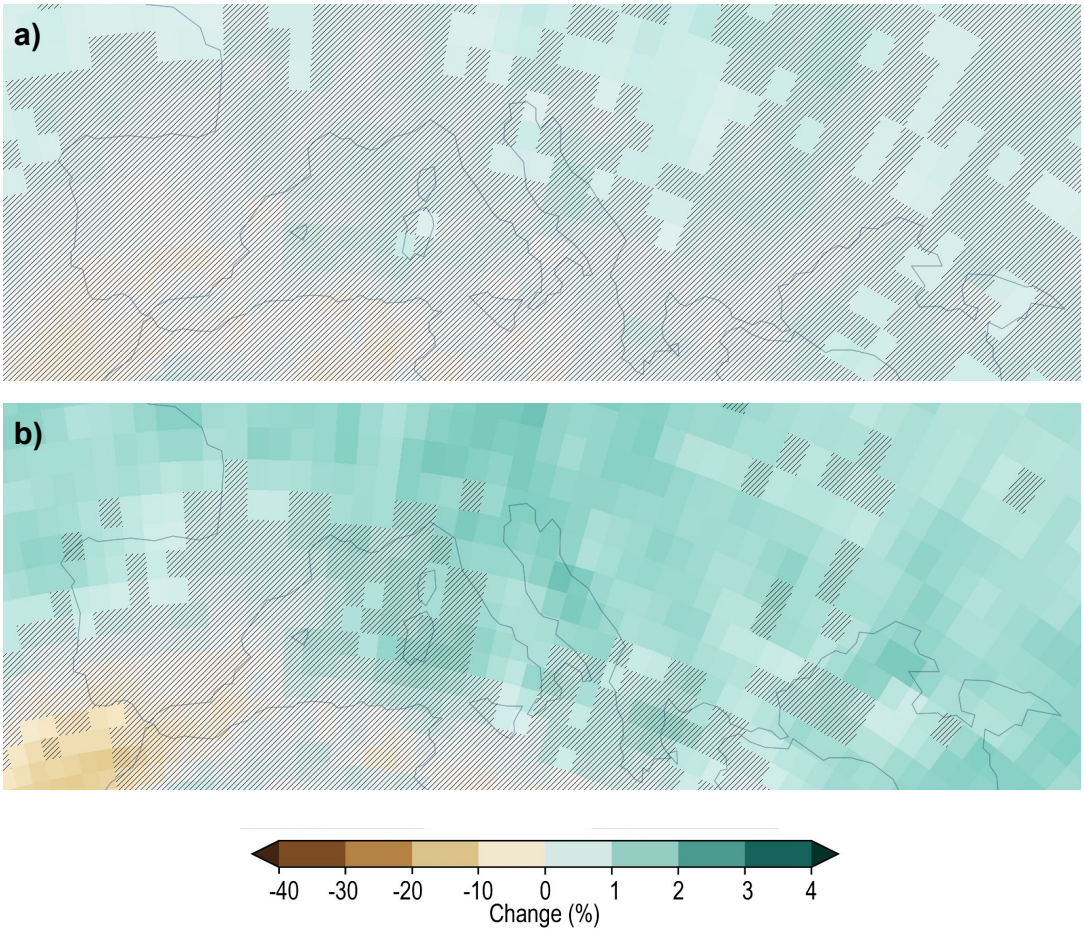

Figure 1.6: Projected changes in annual maximum daily precipitation at (a) 1.5°C and (b) 4°C of global warming compared to the 1850–1900 baseline. Results are based on simulations from the Coupled Model Intercomparison Project Phase 6 (CMIP6) multi-model ensemble under the Shared Socio-economic Pathway (SSP), SSP5-8.5 scenario. The number of simulations included are 33 and 19, respectively for 1.5°and (c) 4°C of global warming. Uncertainty is represented using the simple approach: no overlay indicates regions with high model agreement, where $\geq 80\%$ of models agree on the sign of change; diagonal lines indicate regions with low model agreement, where $< 80\%$ of models agree on the sign of change. Image realized with atlas of [3].

Concerning the future projections of flood events, always following [3], warming of 2 degrees could increase the fraction of global area susceptible to flood hazards (medium confidence). Even if some papers asses that an increase in global warming can lead to an increase in the frequency of high floods in all continents except Europe, more recent results suggest that such assessments have medium confidence at a global scale and low one at a regional one. “In summary, climate projections indicate a larger fraction of land areas to be affected by an increase in river floods in Asia, India, tropical Africa, and North America (medium confidence), while a decreasing in central and eastern Europe and the Mediterranean (high confidence)” [3].

Typically, hydrology-related climate change impact indicators are used to make a risk assessment on a global scale. By following such rationale, [9](Alfieri et al.) present a model to derive a flood hazard map, then in [10](Alfieri et al.) studied the implications of high-end climate scenarios on future hydro-meteorological patterns over Europe, by enhancing the evaluation and visualization of frequency, magnitude and uncertainty of floods events in such scenarios. [11](Alfieri et al.) realized a flood risk assessment in Europe under high-end climate scenarios. Finally, in [12](Alfieri et al.), for a warmer world, global projections of river flood risks and their impact are analysed. By adopting such global-scale models to a local problems, and following the suggested by My climate Risk, an intermediate-complexity flood risk model for adaptation to flooding risk for future climate scenarios is realized by [1](Ruggieri et al.). Since that model was originally structured to estimate the flood risk events for a near term (2011-2040), mid-term (2041-2070) and long-term (2070-2100), this thesis work shows how it could be developed in order to allow it to estimate flood risk events at specific Global Warming Levels (GWLs). This is important because we are changing the question from "what will happen in the next years?", to "what will happen if a certain global warming level is reached?". Since that model is based on open-source data available from climate services Copernicus, local analyses in all the Europe countries can be performed. My part in developing the model involved: writing some codes in python, partial model validation and estimation of flood events impact at different GWLs. Finally, the thesis performs a validation of the model for 3 Italian medium-size catchments, the Panaro, Reno and Secchia rivers, sharing similar geometry and affected by similar precipitation events since they are all enclosed in 44 km.

A model, to describe the earth system, can choose to follow different ways according to how complex the representation must be, i.e. the number of interactions and details degree used; this generates a kind of hierarchy. Models which take into account a low number of processes, with a high degree of interaction between them and with a low degree of detail, are called "conceptual models" (used for long-term climate simulations). Conversely, those that include a high number of processes with a weak reciprocal interaction and a high degree of detail, are called "comprehensive models" (such as GCMs). It is in the middle of the spectrum that intermediate-complexity models find a position, i.e. those models that can select which processes describe, how they interact with each other and with which degree of detail. Although the model here presented exploits the results of a higher-complexity one, it abandons the degree of detail in favour of an inexpensive computational cost, by allowing it to be run on any notebook in circulation today. It is within this framework that the model located, by describing, using statistical tools, phenomena that would require a high degree of detail and number of interactions [13](Claussen et al.).

Chapter 2 introduces some conventions about risk, hazard, exposure, vulnerability and concepts like Disaster Risk Reduction (DRR) and Climate Change Adaptation (CCA). Chapter 3 concerns the methodology followed by the model with some mathematical aspects, a section about the model formulation, the data used by the model and the modelling approach. Chapter 4 is about some python codes that I have made. In Chapter 5, a sensibility test is performed about some assumptions made in Chapter 2, then a model validation is performed through comparison with observed data; after the model undergoes tests concerning the multi-model ensemble used. In the last section of the chapter, an estimation of flooding risk in future scenarios is proposed. In the first section of Chapter 6, there is a brief summary concerning what was made in the previous chapters, while in the second section the results are discussed with some remarks about the potential approach and future development of the model.

Chapter 2

Risk assessment methodologies

In this chapter, the meanings of risk, hazard, exposure, and vulnerability and how they interfaced with each other will be discussed to understand how to describe extreme events and to perform Disaster Risk Reduction (DDR) and Climate Change Adaptation (CCA).

2.1 Risk, hazard, exposure and vulnerability

The IPCC framework for the assessment of the risk associated with extreme hydrometeorological event partition the risk into three components: hazard, exposure and vulnerability. That are respectively the probability and magnitude of that event (*Hazard*), the fraction of environment, human and economic activities (asset category) susceptible to that event (*Exposure*), and the magnitude order of damage suffered by asset category exposed (*Vulnerability*). Indeed in this framework, the risk is conceptually defined as the "result of dynamic interactions between climate-related hazards with the exposure and vulnerability of the affected human or ecological system to the hazards"[2]. In this work, we will refer to flood events of rivers, events in which the river banks are not able anymore to constrain the streamflow resulting in leakage of water, i.e. inundation. Thereby, each flooding event will be described in terms of a river discharge, which depends on precipitation events, and flood height, which is our hazard that we will link to river discharge. The fraction asset category affected by an event, will depend on the flood height, while the damage suffered, in economic terms, depends also from asset category typology interested [12](Alfieri et al.).

One of the major impact drivers of climate change is the modification of the frequency of extreme events. According to [10] (Alfieri et al.), in Europe, flood events projections will be characterized by an increase in frequency and magnitude. This implies an increase of flood risk, and that can be estimated in terms of an increase in the population exposed and expected economic damage caused by floods. How much the frequency will increase and how severe such events will be, depends on the shared socioeconomic pathways (SSP) and Representative Concentration Pathway (RCP). As reported by [11](Alfieri et al.) and shown in Fig. 2.1, a scenario $RCP8.5$ (high emission scenario), which is compatible with $SSP3$ and $SSP5$ (Regional Rivalry and Fossil-fueled Development), will lead to an estimate of the population annually affected between 540,000 and 950,000 in 2080 and expected damage of flooding ranging from 20 to 100 *Beuro* per year.

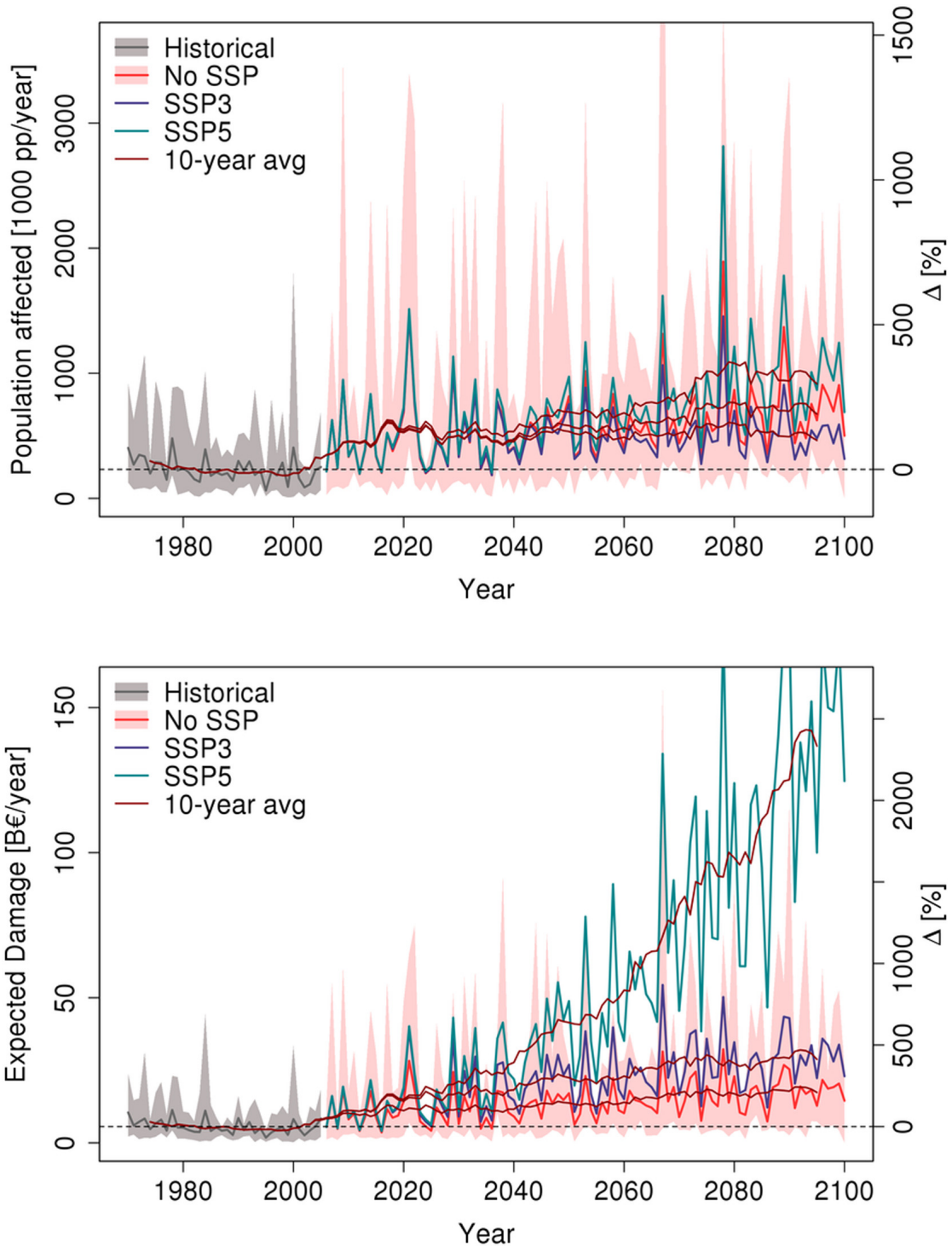

Figure 2.1: Simulated damage and population affected per year and relative change from the baseline scenario (Europe-wide aggregated figures). Future scenarios include no SSP (with ensemble spread in pink), SSP3, and SSP5, together with their 10-years moving average. Image taken from [11].

In this thesis the following definitions are adopted: *Risk Assessment* defined as "the qualitative and/or quantitative scientific estimation of risks" and *Risk Management* defined as "plans, actions, strategies or policies to reduce the likelihood and/or magnitude of adverse potential consequences, based on assessed or perceived risks" [2]. The reduction of the likelihood and/or magnitude is performed by *Risk Mitigation* defined

as "the lessening of the potential adverse impacts of physical hazards (including those that are human-induced) through actions that reduce the exposure and vulnerability" [14] and *Climate Change Mitigation*, actions like reducing the sources or improve the sinks of greenhouse gases [15]. This last concept falls in the so-called "top-down" approach, which is an ensemble of measures performed on a global scale, that through the coordination of all the countries try to respect the Paris agreement target of $1.5°C$.

2.2 Disaster Risk Reduction and Climate Change Adaptation

Since a "top-down" approach was pursued to perform mitigation to climate change, and this proved unsuccessful, it was necessary to introduce a new one, the "bottom-up" approach, in which "climate change is just one factor among many to consider" [5](Rodrigues et al.) What this approach pursues is the adaptation to climate change, which for we mean "the process of adjustment to actual or expected climate and its effects, in order to moderate harm or exploit beneficial opportunities" [2]. For a positive outcome in the "fight" against climate change, both mitigation and adaptation must be taken into account and this implies that concerted "top-down" and "bottom-up" actions are needed.
Disaster Risk Reduction (DRR) and Climate Change Adaptation (CCA) are two approaches that aim reduce risk associated with hydro-meteorological hazards. DRR measures try to decrease the impact of future disaster events by acting on the exposure and vulnerability components of risk [14]. In a contest of flood event, acting on the exposure means, for example, reducing the population affected, acting on vulnerability could mean to reorganized the spatial configuration of asset categories since not all of them suffered the same damage for a given flood event. CCA tries to provide a way to better understand the actual and future climate conditions to perform efficient measures of adaptation. In the context of flood events means to characterize correctly frequency and magnitude, if they will increase or decrease and if a global pattern is recognizable. In this regard, for example, [7](Dankers et al.) has found different mechanisms from which events of flooding can arise. Since, typically, the meteorological forcing that causes flood events are the annual maximum 5-day accumulated rainfall, in warmer earth, flood events will increase in western Europe [16](Maria Carmen Llasat et al.). A different mechanism drives the flood events in northeast Europe, the snow melting in spring, which, for a warm earth will decrease [7](Dankers et al.). The result is that, in the future, flood events in northeast Europe will become rare, therefore they will not need adaptation measures. In order to make adaptation measures more efficient, a regional analysis like these must be performed for each extreme event to identify in which regions should are necessary and in which not. Both DDR and CCA try to act on another important aspect, the improving of *Resilience*, which is defined as "the capacity of interconnected social, economic and ecological systems to cope with hazards event, trend or disturbance, responding or reorganizing in ways that maintain their essential function, identity and structure"[2]. Therefore, more effort must be turned towards the realization of flexible tools which, by using open-source data from climate services, allow us to assess the risk in future climate scenarios. Another aim is the quantitative estimate of some possible adaptation measure which acts on hazard, exposure and vulnerability in order to find which of such measure lead to more effective adaptation; is in this direction that this model tries to work.

Chapter 3

Methodology

In the first section of this Chapter, 3.1, the Gumbel distribution is discussed. In section 3.2, the rationale followed by the model is given, with a focus on the system of equations on which the model is based. In the sections 3.3 and 3.4, the datasets used and the workflow of the model are shown, while in the last part of the section 3.4 the concept of Areas of Influence followed is presented.

3.1 Type-I generalized extreme value distribution

From [17], the cumulative distribution function (CDF) of the Gumbel distribution is

$$F(x) = e^{-e^{-(x-\mu)/\beta}} \tag{3.1}$$

or equivalent, by defining the reducing variable

$$y = \frac{x-\mu}{\beta}$$

we obtain the compact form

$$F(x) = e^{-e^{-y}}. \tag{3.2}$$

With CDF we can define the probability of occurrence of an event equal to or smaller than a threshold value x_T

$$F(x_T) = P(x < x_T) \tag{3.3}$$

as a consequence the probability of occurrence of an event larger than a threshold value x_T is

$$P(x \geq x_T) = 1 - P(x < x_T). \tag{3.4}$$

The return period is defined as the average time or an estimated average time between two events with a magnitude equal to or larger than a threshold value. Analytically is defined as the reciprocal of the probability (3.4) written as

$$T = \frac{1}{P(x \geq x_T)} = \frac{1}{1 - P(x < x_T)}. \tag{3.5}$$

Thanks to (3.5) and (3.3) we find that

$$F(x_T) = \frac{T-1}{T}. \tag{3.6}$$

Solving (3.2) for y_T

$$y_T = -ln\Big[ln\Big(\frac{1}{F(x_T)}\Big)\Big], \tag{3.7}$$

that we can rewrite, thanks to (3.5), as

$$y_T = -ln\Big[ln\Big(\frac{T}{T-1}\Big)\Big]. \tag{3.8}$$

Finally by substituting the RHS of (3.1) into (3.8)

$$\frac{x_T - \mu}{\beta} = -ln\Big[ln\Big(\frac{T}{T-1}\Big)\Big], \tag{3.9}$$

and solving for T

$$T(x_T) = \frac{e^{-e^{(x-\mu)/\beta}}}{e^{-e^{(x-\mu)/\beta}} - 1}, \tag{3.10}$$

The equation (3.10), (3.8) and (3.1) will be rearranged in order to describe flooding events.

3.2 Model formulation

The model aims to give an estimate, with more accuracy as possible, about the risk of flooding events in future possible degree scenarios, by referring to the statistic of variables later on defined. As already long-established, the risk $R = hev$ is defined as the product of hazard h, exposure e, and vulnerability v. The input of the model is the river discharge (Q) simulated for future degree scenarios and the flooding height statistics in the present climate. In order to determine the future risk of flooding events, some fundamental hypothesis, soon implemented, will allow us to compute the statistic of flooding height in future climate scenarios. The vulnerability v and exposure e are taken into account in the model respectively through, empirical hazard-damage functions and satellite-based or modelled land cover data, both of them will be thoroughly described in Chapter 3.3. The projection of river discharge and the flooding height statistics in the present climate used by the model are treated in the same section.

The fundamental hypothesis of the model is to assume that the probability of a flooding event, characterized by a flooding height h, is

$$p(h_i)dh_i = g(Q(r_i))dQ, \tag{3.11}$$

where r_i is a river network point, and i identifies a domain point subjected to flooding events. Through the concept of Area of Influence, we assume that the flooding height in the point i is caused only by the discharge in the river network point r_i; that computational procedure is described in Chapter 3.4. In that way, the statistic of the flooding height is ascribable to the statistic of return periods of discharge Q. This means that the probability of an event, characterized by a flooding height h, with a magnitude equal to or smaller than a given value H is

$$P(h \leq H) = \int_0^H p(h_i)dh_i = \int_{q_0}^{q_1} g(Q(r_i))dQ, \tag{3.12}$$

this equality, which is a consequence of (5.1.1), must be verified for every catchment considered. Rearranging eq.(3.10) in terms of flooding variables

$$T_m^n(r) = g_m(Q(r)) = \frac{e^{-e^{(Q(r)-\mu_m(r))/\beta_m(r)}}}{e^{-e^{(Q(r)-\mu_m(r))/\beta_m(r)}} - 1}. \tag{3.13}$$

"The simulated high flow events are defined by taking the maxima of a daily time series. For each model chain m we can the define a sequence, for $n = 1, ..., N(m)$, of $N(m)$ modelled flood events identified by the return period T_m^n" [1](Ruggieri et al.).

By taking into account (3.1), $Q(r)$ is given by

$$Q(T, r) = \beta_m(r)y(T) + \mu_m(r), \tag{3.14}$$

this fit, through which $\beta(r)$ and $\mu(r)$ coefficients are computed, is performed by considering the return periods $T = 2, 5, 10, 50$ years. In the same way, the flood height of the n-th event simulated by the m-th model is computed through the following fit

$$h_i(T_m^n) = \gamma_i y(T_m^n) + \epsilon_i, \tag{3.15}$$

by considering the return periods $T = 10, 20, 50, 100, 200, 500$ years. By implementing the hypothesis (5.1.1), we are able to perform a projection of flooding heights

$$h_i(T_m^n) = \gamma_i y(T_m^n(r_i)) + \epsilon_i. \tag{3.16}$$

Following [10](Alfeiri et al.) and [1](Ruggieri et al.) a flood protection function is introduced in order to label with T_m only the annual maximum river discharge which causes a flood event.

$$f_p(T) \equiv \theta(T - T_P(r)). \tag{3.17}$$

In this regard the condition $T_m > T_p$ must be satisfied, where T_p is the return periods of the streamflow for which the protection systems allow to avoid the flooding event, such values are provided in FLOPROS(see Chapter 3.3). Following [1] we define the damage function as

$$D = D_c^{max} d_c(h), \tag{3.18}$$

where D_c^{max} is a damage normalization factor which differs for each asset category c and $d_c(h)$ is a function which expresses the value of the damage as a function of flooding height h (see Chapters 3.3 and 4). Therefore, for each river network point r, eventually connected to a domain point i susceptible to flooding events, we define a damage-frequency curve [1] that associate to a local streamflow event with return period T in r, the total damage of that event

$$D(T, r) = \sum_c D_c^{max} \sum_i d_c(h_i(T))\delta_{c,c_i}\delta_{r,r_i}, \tag{3.19}$$

where $\delta_{c,c_i} = 1, \delta_{r,r_i} = 1 \iff c = c_i, r = r_i$ otherwise $\delta_{c,c_i} = 0, \delta_{r,r_i} = 0$. Following [1] the simulated expected damage can then be computed

$$R(r) = \frac{1}{M} \sum_{m=1}^{M} \frac{1}{N} \sum_{n=1}^{N} D(h_i(T_m^n), r). \tag{3.20}$$

Finally the model equation can then be summarised by the following system of equations

$$\begin{cases} T_m^n(r) = g_m(Q(r)) = \dfrac{e^{-e^{(Q(r)-\mu_m(r))/\beta_m(r)}}}{e^{-e^{(Q(r)-\mu_m(r))/\beta_m(r)}} - 1} & (3.21) \\ h_i(T) = (h_i^1 y(T) + h_i^0) f_p(T) & (3.22) \\ D(T,r) = \sum_{i,c} D_c^{max} d_c(h_i(T)) \delta_{c,c_i} \delta_{r,r_i} & (3.23) \\ R(r) = \dfrac{1}{M} \sum_{m=1}^{M} \sum_{n=1}^{N(m)} D(T_m^n, r) & (3.24) \end{cases}$$

Where m is referred to the ensemble member having size M, n is the high flow event simulated by the ensemble member, $N(m)$ is the number of events simulated by the member m, T is the return period, Q is the streamflow, h_i is the flood height in i, $\beta_m(r)$, $\mu_m(r)$, h_i^0 and h_i^1 are the parameter of the linear fit, $f_p(T)$ is the local protection function, c is a land cover category, D_c^{max} is a damage normalization factor associated to the asset category c, $d_c(h_i)$ is the damage as a function of flooding height h_i.

3.3 Data

Adapted from [1](Ruggieri et al.), data used by the model are summarised in Tab. 3.1. Data of flood height statistics in present climate are obtained from [18](Dottori et al.) for 6 return periods (10, 20, 50, 100, 200, 500 years). Land cover data are obtained from the CORINE land cover [19](György Büttner et al.)) of the Copernicus Land Monitoring Service. Empirical damage functions from the "Global flood depth-damages functions" are available from [20](H. Huizinga et al.). To account for flood protection measures that are not represented in hydrodynamic models applied to obtain the flood hazard maps we use modeled FLOod PROtection Standards (FLOPROS) that are made available by [21](Scussolini et al.). This dataset provides return periods handled by protection measures.

Dataset name	Reference period	Variables	Resolution	Data type
Hydrology-related climate impact indicators	Baseline:1971-2000 Near term:2011-40 Mid term: 2041-70 Long term:2071-2100	Streamflow	5 Km	Hazard
River flood hazard maps for Europe and Mediterranean Basin region	1990/2016	Flood height (m)	100m	Hazard
CORINE Land Cover	2018	Land cover	100m	Exposure
Global flood depth-damages functions	2010	Damages (2010 $Euros/m^2$)	Continent	Vuln--rability
FLOod PROtection Standards	2016	Return period (years)	Administrative	Vuln--rability height

Table 3.1: Overview of datasets used in this study. The first column indicates the official name of the dataset, the second column indicates the reference time frame of the dataset, the third column shows the variables used, the fourth column is the nominal spatial resolution and the last column classifies the datasets used into the categories of hazard, exposure and vulnerability (adapted from [1](Ruggieri et al.))

From the dataset "Hydrology-related climate impact indicators" we select the daily river discharge or streamflow ($m^3 s^{-1}$) on grid resolution ($5Km$) as changes over three future periods for three RCPs(Representative Concentration Pathways), and three-degree

scenarios for a global mean temperature increase of 1.5, 2.0 and 3.0 °C above pre-industrial conditions [22]. The streamflow values are given by projections of the EURO-CORDEX (EUR11) ensemble, realized by using three different General Circulation Models (GCMs), where each of them is downscaled to $12.5km$ through Regional Climate Models (RCMs). Such model chain is bias adjusted by using EFAS-Meteo data set [23]. The bias is defined as "systematic deviations from the reference data used for impact modelling, including deviation due to discrepancy in the spatial resolution" [22]. Therefore, "the bias correction is a necessary step when meteorological data from climate models are to be employed as driving data for impact models" [22]. In our case, the impact models forced by EUR11 are hydrological models ensemble composed by, E-HYPEcatch multi-model system $(0, 11°)$, E-HYPEgrid $(5Km)$, and VIC-WUR $(5Km)$, the last two are the ones that will be used. Since the data set used, for the bias adjustment (EFAS-meteo), start record in 1990 the reference period is $1990 - 2018$. The bias adjustment is performed by calibrating a "transfer function" on the reference period, which is then applied to the time series $1971 - 2100$ of the multi-model ensemble for temperature and precipitation variables. Then, a transfer to the standard calendar for HadGEM-ES is performed. Finally, a transferring bias adjustment to sub-daily time steps only for temperature is implemented (for more detail see [22]).

GCM	RCM	Hydrological	ENS. Members	Scenarios (RCP)
EC-EARTH	CCLM4-8-17	VIC-WUR and E-HYPERgrid	1	2.6, 4.5, 8.5
EC-EARTH	RACMO22E	VIC-WUR and E-HYPERgrid	1	2.6, 4.5, 8.5
EC-EARTH	RCA4	VIC-WUR and E-HYPERgrid	1	2.6, 4.5, 8.5
HadGEM2-ES	RCA4	VIC-WUR and E-HYPERgrid	1	2.6, 4.5, 8.5
HadGEM2-ES	RACMO22E	VIC-WUR and E-HYPERgrid	1	2.6, 4.5, 8.5
MPI-ESM-LR	RCA4	VIC-WUR and E-HYPERgrid	1	2.6, 4.5, 8.5
MPI-ESM-LR	REMO2009	VIC-WUR and E-HYPERgrid	2	2.6, 4.5, 8.5

Table 3.2: Models used for climate projections, adapted from [1].

Only for MPI-ESM-LR GCM, we can take into account two different realizations, so we use all available 14 model chains to form a multi-model ensemble with 16 members for the RCP 8.5 ("High pathway for which radiative forcing reaches greater than 8.5 Wm^{-2} by 2100 and continues to rise for some amount of time, assuming constant emissions after 2100 and constant concentrations after 2250" [14]). All the following results, which depend on multi-model ensemble projections, will label as CMIP based, while the results based on reference data will label as EFAS based.

Data used for river streamflow validation in Chapter 5.1.2 are reported in Tab. 3.3, obtained from some italian authorities like AIPO(Agenzia Interregionale per il fiume Po, Auorità di Bacino (AdB) fiume Reno and Comune di Marzabotto.

	Panaro	Reno Casalecchio 1	Reno Casalecchio 2	Reno Marzabotto 1	Reno Marzabotto2	Secchia
$Q_{20}(m^3s^{-1})$	1030		1833		1338	1350
$Q_{25}(m^3s^{-1})$		1477		1011		
$Q_{30}(m^3s^{-1})$		1541		1135		
$Q_{50}(m^3s^{-1})$			2099		1536	1600
$Q_{100}(m^3s^{-1})$	1270	1981	2298	1403	1685	1900
$Q_{200}(m^3s^{-1})$	1480	2280	2421	1577	1776	2050
$Q_{500}(m^3s^{-1})$	1660		2773		2038	2250
Drainage basin area km^2	742	1061	1051	1061	1051	1341

Table 3.3: River discharges Q_i, where i is the return period in year, provided respectively by authorities AIPO(Agenzia Interregionale per il fiume Po)[24],[25] for Panaro and Secchia rivers, Auorità di Bacino fiume Reno [26] for Reno Casalecchio 1 and Reno Marzabotto 1 and Comune di Marzabotto [27] for Reno Casalecchio 2 and Reno Marzabotto 2.

All lack of data in Tab.3.3, are due to missing information from the authorities from which are taken. The data provided by AIPO-Secchia [25] are obtained from observed data with Hydrologic Modeling System (HEC-HMS), while for AIPO-Panaro [24], are not specified from which procedure they come. With regard to AdB [26], the data are obtained from a hydrologic model based on De Saint Venant equations in complete form, while the ones obtained from Comune di Marzabotto [27] are based on rationale cinematic methods.

3.4 Workflow of the model

The workflow is shown in Fig. 3.1 where EURO-CORDEX EUR11, which is bias adjusted with EFAS-meteo, force an ensemble of hydrological models composed by E-HYPEgrid, and VIC-WUR to compute the statistical of river discharge $Q(T)$ that lead to obtaining the statistic of flood height $H(T)$ in future scenarios. After, with CORINE land cover, Global flood depth-damages functions and FLOPROS the damage cost in future scenarios is computed. Such damages can be confronted with the ones computed in present climate by using river food hazard maps and the same auxiliary functions.

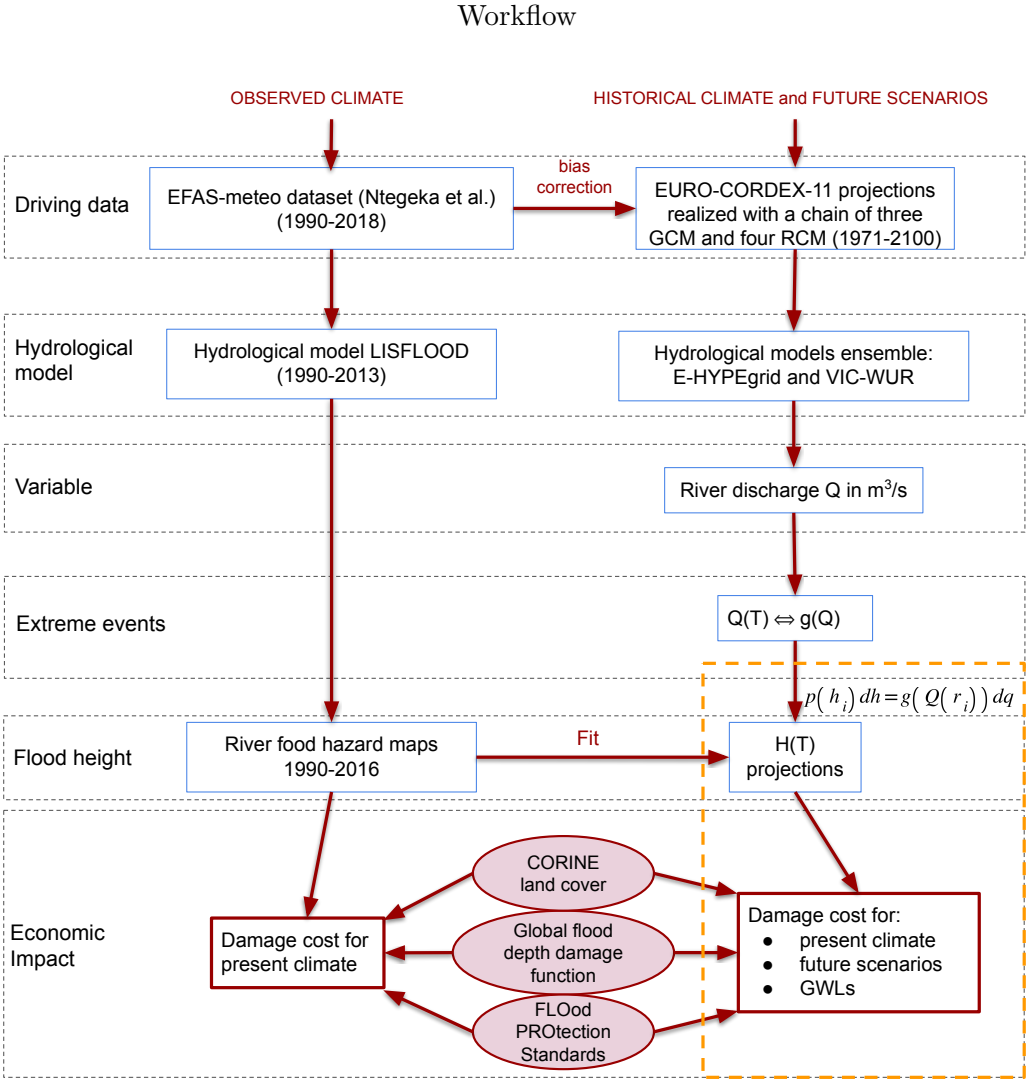

Figure 3.1: Schematic representation of approach to estimate the damage cost in present climate and future climate scenario. The projections are taken from EURO-CORDEX EUR 11 ensemble, performed by a models chain which consists of three different global climate models (GCMs) downscaled through four different regional circulation models (RCMs). Such ensemble force HYPEgrid and VIC-WUR hydrological models. The dashed orange box shows the approach proposed by this work. More details, about datasets, are reported in Chapter 3.3.

Since the river discharges in Tab. 3.3 are peak values, while the ones computed by models CMIP based are daily averaged, a conversion is necessary to make a validation of the model. This conversion is performed through the empirical formula [28]

$$Q_{peak} = Q_{dailymean} \cdot F \; with \; F = 16 \cdot A^{-0.19}$$

where A is the drainage basin area reported in in Tab. 3.3.

Another important step is the merging of $100m$ resolution maps of flooding height (finner shading in Fig. 3.2) with the 5km resolution maps of streamflow (coarser shading Fig. 3.2). To realize that aggregation, the definition of Areas of Influence (AoI) is used.

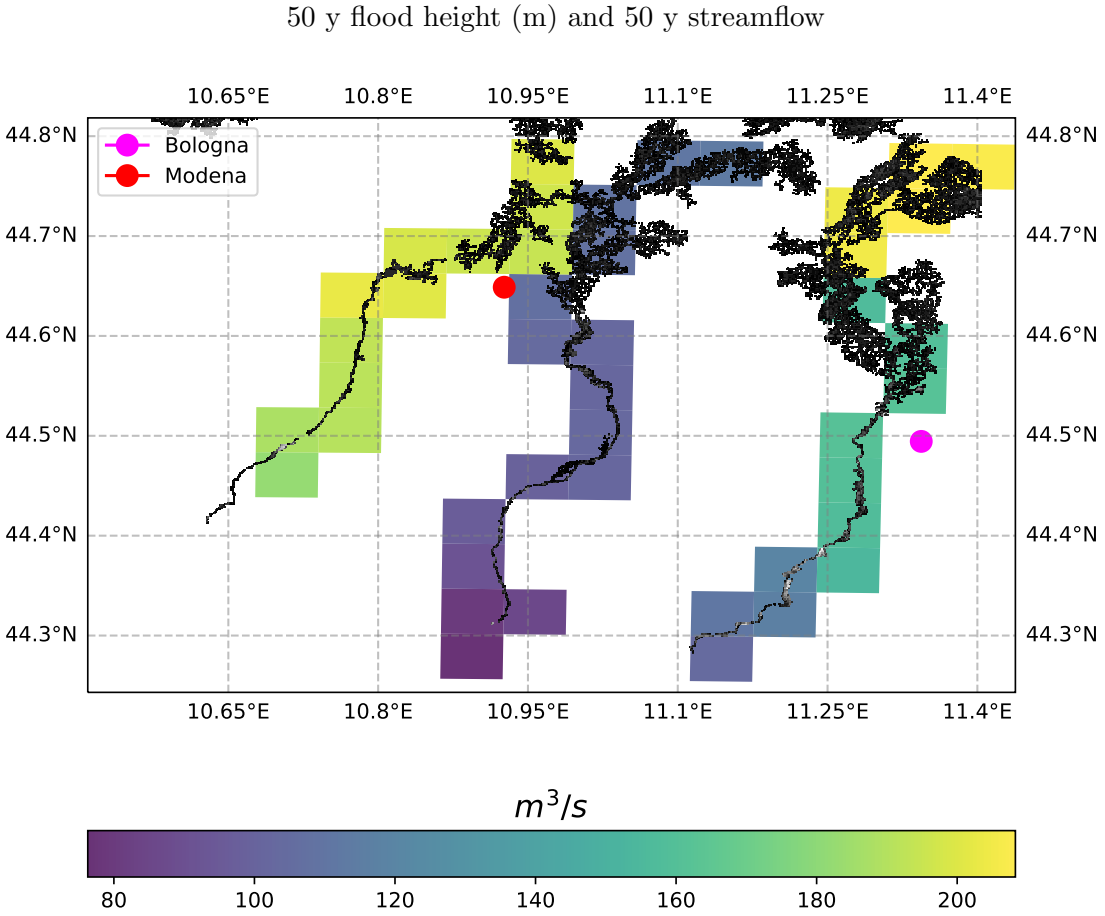

Figure 3.2: Simulated flood statistics in the domain of the rivers, the shading on the coarser scale indicates the 50-year streamflow $m^3 s^{-1}$ while the shading at a finer resolution shows the 50-year flood height.

The rationale of AoI, implemented in this model, is the assumption that the river network point, which determines the flooding height in a domain point, is the nearest one to such domain point. In this way, we can link, uniquely, which point of the river network determines the flooding height in a certain domain point during a flood event. The result of that procedure is a domain division in Areas of Influence. A graphic example of that procedure, respectively for Reno and Secchia rivers, is shown in Fig. 3.3. The domain regions not coloured are the regions not interested in a flooding event of that river network.

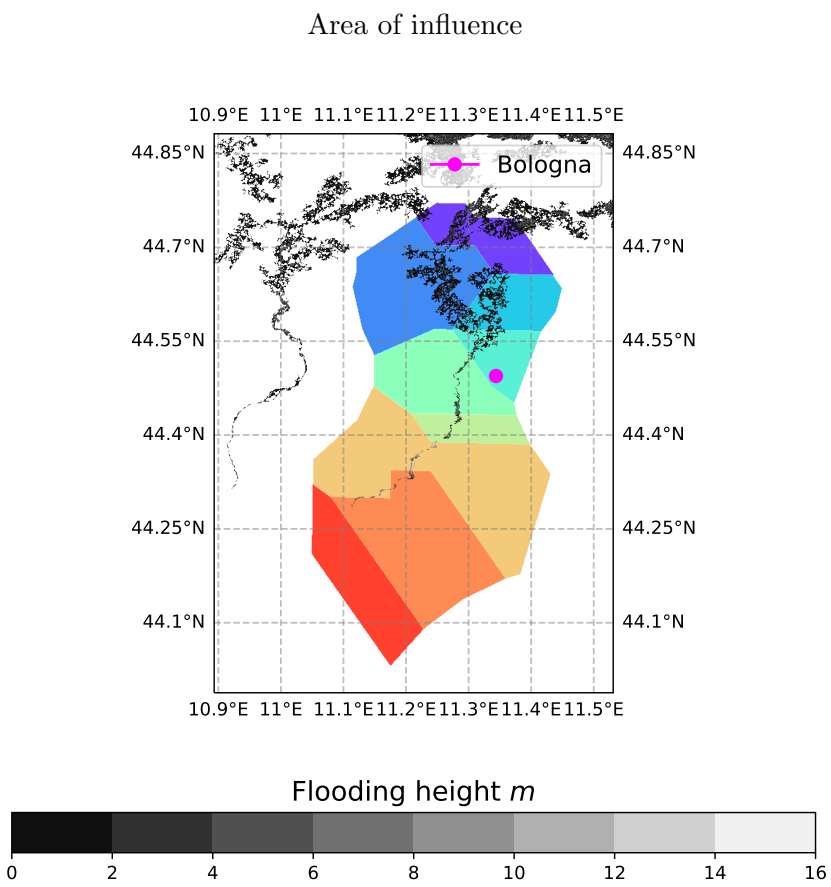

(a) Reno area of influence

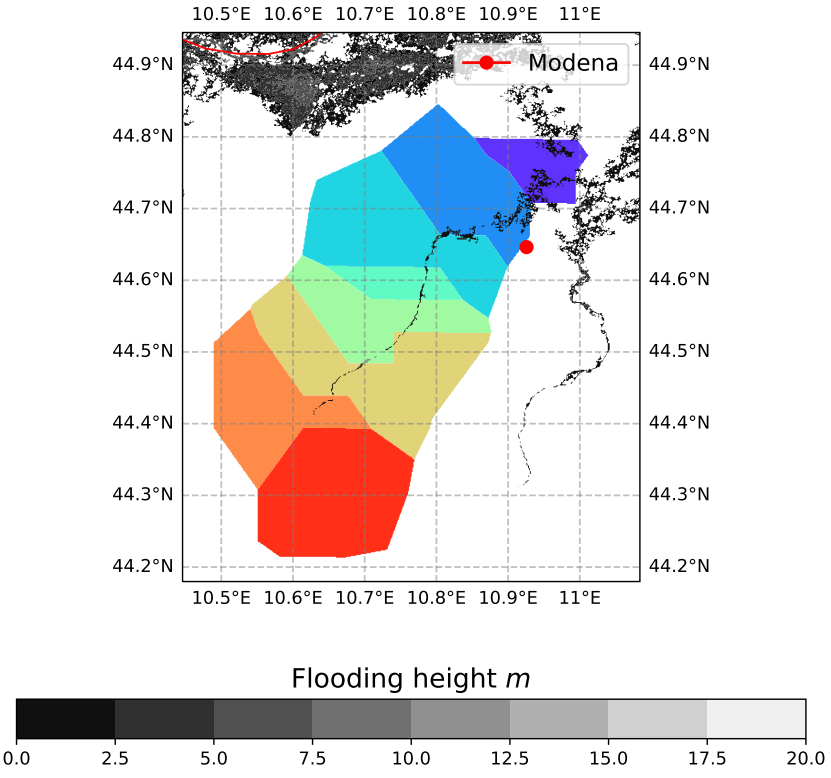

(b) Secchia area of influence

Figure 3.3: Areas of flood influence (coloured region) at 100 m resolution for Reno and Secchia river network, (a) and (b) respectively, for a 50 years return period events.

Chapter 4

Model development

In this Chapter, the outline code will be shown with some code extracts which constitute my contribution to the realization of this model. In order to summarize the procedure of the model, Fig. 4.1 represent the outline followed by the code, in which the most important data, variable and function used are reported.

Code outline

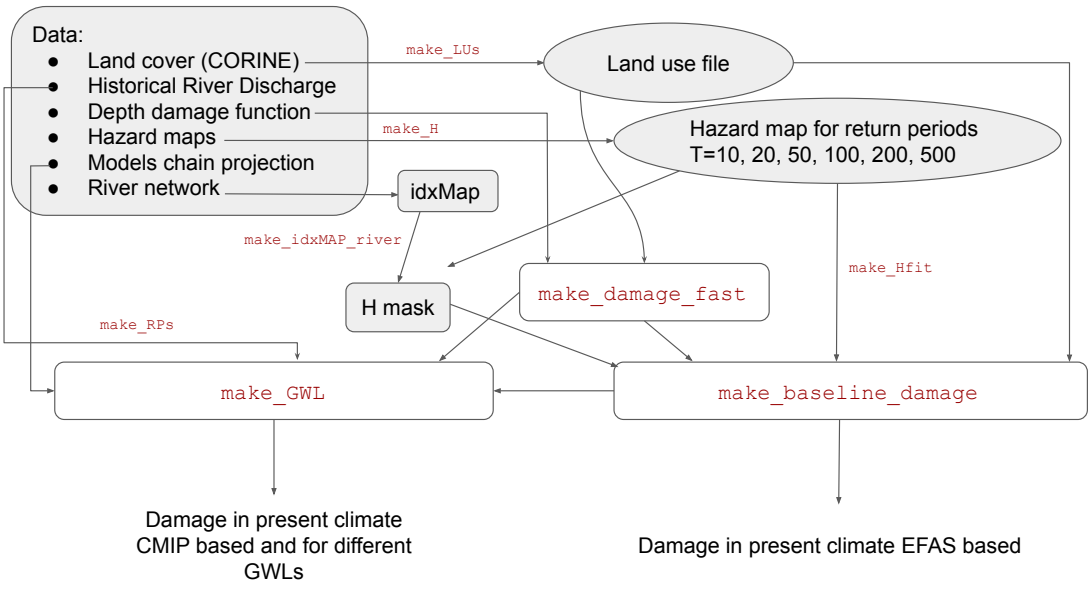

Figure 4.1: Code outline followed by the model. The red writings are all functions that are collected into a $Risk - function$ python script; such functions, are taken as input, data or output of other functions. The grey-shaded box represents the data taken in the input and/or the output of the function. Other important variables, dictionaries and lists concerning GCM, RCM, GWLs, damage function and land use parameters are collected into a $Risk - dict$ python code. Details about functions are provided in appendix A.

One of the key points of the model is to determine the damage associated to a flooding height by taking into account the asset category typology interested by flooding event. Six asset categories have been identified, which are: agriculture, residential, commercial, industrial, roads and transport. By following [20], a flood damage fraction is given for each asset category (Damages in Listing 3.1) in function of flooding heights (Hdamage in Listing 3.1).

```
import numpy as np
import matplotlib.pyplot as plt


Damages={'agri':np.array([0.00,0.30,0.55,0.65,0.75,0.85,0.95,1.00,1.00]),
         'resi':np.array([0.00,0.25,0.40,0.50,0.60,0.75,0.85,0.95,1.00]),
         'comm':np.array([0.00,0.15,0.30,0.45,0.55,0.75,0.90,1.00,1.00]),
         'indu':np.array([0.00,0.15,0.27,0.40,0.52,0.70,0.85,1.00,1.00]),
         'roads':np.array([0.00,0.25,0.42,0.55,0.65,0.80,0.90,1.00,1.00])
    ,
         'trans':np.array([0.00,0.32,0.54,0.70,0.83,1.00,1.00,1.00,1.00])
    }
Hdamage=np.array([0,0.5,1,1.5,2,3,4,5,6])
```

Listing 4.1: Asset category and max damages

In order to take into account the fact that the same flooding height cause different damages depending on the asset category affected, the flood damage in terms of *Euros* m^{-2} can be obtained by multiplying the previous flood damage fraction with MaxDamages citeflooddamagefunction values reported in the following list.

```
MaxDamages={'agri':0.22,'resi':148,'comm':308,'indu':251,'roads':21,'
    trans': 625}
```

Listing 4.2: Max Damages

Since such data are referred only for 9 flooding heights, in order to determine the damage for a generic flooding height value, an interpolation is performed by the following listing.

```
from scipy.interpolate import UnivariateSpline

x=Hdamage
newH=np.linspace(0,6,80)
y=Damages['agri']
spl= UnivariateSpline(x, y)
Nagri=spl(newH)
y=Damages['resi']
spl= UnivariateSpline(x, y)
Nresi=spl(newH)
y=Damages['comm']
spl= UnivariateSpline(x, y)
Ncomm=spl(newH)
y=Damages['indu']
spl= UnivariateSpline(x, y)
Nindu=spl(newH)
y=Damages['roads']
spl= UnivariateSpline(x, y)
Nroads=spl(newH)
y=Damages['trans']
spl= UnivariateSpline(x, y)
Ntrans=spl(newH)
```

Listing 4.3: Damage function interpolation

The for cycle in the following listing is introduced by myself to avoid that, once the asymptotic damage value is reached, do not vary anymore.

```
Nagri[Nagri>1]=1
Nresi[Nresi>1]=1
Ncomm[Ncomm>1]=1
Nindu[Nindu>1]=1
Nroads[Nroads>1]=1
Ntrans[Ntrans>1]=1

```

```
#For cycle
for i in range(len(newH)-1):
  if Nagri[i]==1:  Nagri[i+1]=1
  if Nresi[i]==1:  Nresi[i+1]=1
  if Ncomm[i]==1:  Ncomm[i+1]=1
  if Nindu[i]==1:  Nindu[i+1]=1
  if Nroads[i]==1: Nroads[i+1]=1
  if Ntrans[i]==1: Ntrans[i+1]=1
```

Listing 4.4: Damage function interpolation

Fig. 4.2 represent graphically the two damages function computed in the previous listings. From the figure at the bottom of Fig. 4.2 is easy to see that, for a given flooding height, the event cause different damages depending on the asset category exposed; the transport appears to be the one more vulnerable compared to others.

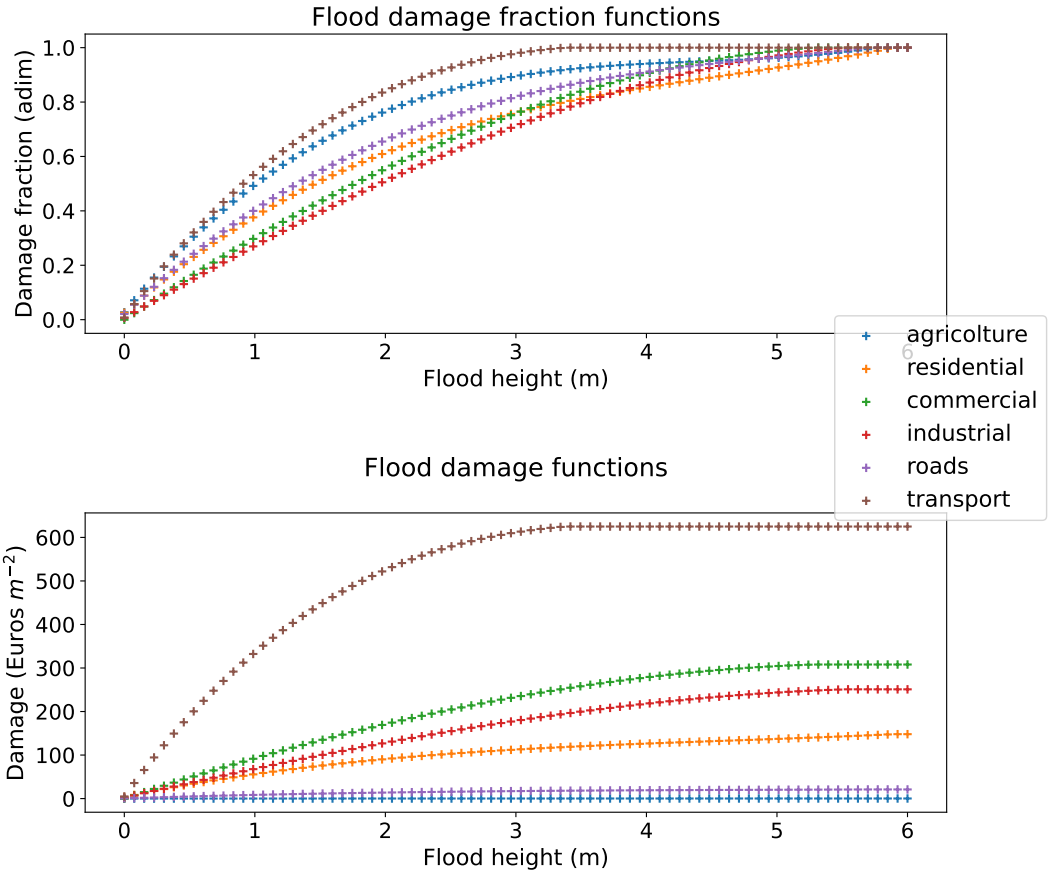

Figure 4.2: Top) Flood damage fraction functions obtained from an interpolation performed by scipy.interpolate.UnivariateSpline python function in which 80 points are used for a flood height which came from 0 to 6 meters. Bottom) Flood damage functions are obtained from the fraction functions by multiplying them for max damage factors (cite).

To compute the damage in present climate (baseline) and for a given GWL, a python Global Warming Level function is written. In the first part of the listing variables elsewhere calculated are imported and then others are introduced.

```
import numpy as np
```

```
2
3 def make_GWL(red,xN0,yN0,run,method=None,damage_curve='load',shift=0,
    shifty=0):
4     from Risk_functions import make_baseline_damage,load_all
5     from Risk_dict import INDIR,OUTDIR,DATADIR,file_LU,times,models,
    FILESrp,nts,lista,years,gwls,gwl
6     from NAMELIST import exp
7     import numpy as np
8
9     Hfit1,Hfit0,x,y,xC,yC,LU,rm_LU,Xh,Yh,idxMAP_river,=load_all(INDIR,
    OUTDIR)
10    out_baseline=np.zeros([len(models)])
11    out_1=np.zeros([len(models)])
12    out_2=np.zeros([len(models)])
13    out_3=np.zeros([len(models)])
14    out_baseline_NBS=np.zeros([len(models)])
15    out_1_NBS=np.zeros([len(models)])
16    out_2_NBS=np.zeros([len(models)])
17    out_3_NBS=np.zeros([len(models)])
18    Hmask=((idxMAP_river[:,:,0]==xN0)*(idxMAP_river[:,:,1]==yN0))
```

Listing 4.5: Import variable

In the first part of the following listing, the logical condition if is introduced in order to perform a sensitivity test concerning Areas of Influence, whose results are reported in Chapter 5.1.1.

```
1     if method=='sensitivity':
2         print('Using wrong Q for sensitivity')
3         xN0fake=xN0-shift
4         yN0fake=yN0-shifty
5     else:
6         xN0fake=xN0
7         yN0fake=yN0
```

Listing 4.6: Logical condition if

The following listing computes the damage through the function *np.trapz* for the present climate. Then, a for cycle scroll through all sixteen models and introduce the *Qprotection* variable, which is the one that takes into account the fact that a flooding event, to be defined as such, must be characterized by streamflow greater than a threshold value.

```
1 rp_x=0
2 damage_rel=0
3 Damage_x=0
4 out_obs=0
5 if Hmask.sum()>0:
6      if damage_curve=='compute':
7          print('Compute and save damage_rel and rp_x')
8          damage_rel,rp_x=make_baseline_damage(xN0,yN0,nts)
9          np.save(INDIR+'rp_x_'+str(xN0)+'_'+str(yN0)+'.npy',rp_x)
10         np.save(INDIR+'damage_rel_'+str(xN0)+'_'+str(yN0)+'.npy',
    damage_rel)
11     else:
12         damage_rel=np.load(INDIR+'damage_rel_'+str(xN0)+'_'+str(yN0)+'.
    npy')
13         rp_x=np.load(INDIR+'rp_x_'+str(xN0)+'_'+str(yN0)+'.npy')
14     Damage_x=-np.log(np.log(rp_x/(rp_x-1)))
15     out_obs=np.trapz(damage_rel,-1/rp_x)
16     m=0
17     for model in models:
18         DIR=DATADIR+'/CMIP5/merged_yearmax/'
19         FILErcp=DIR+'merged_'+run+'_'+model+'.nc'
```

```
20          FILE=DIR+'merged_'+model+'.nc'
21          DIRrp=DATADIR+'/CMIP5/RPs/'
22          FILErp=FILESrp[model]
23          lon,lat,rdis,rp2,rp5,rp10,rp50,rdisrcp=read_model(FILE,FILErp,
    FILErcp,DIRrp)
24          Fit=make_RPs_new(xN0fake,yN0fake,rp2,rp5,rp10,rp50)
25          Qprotection=-np.log(np.log(49.88/(49.88-1)))*Fit[0]+Fit[1]
```

Listing 4.7: Damage in present climate

The following listing, which is nested in the previous for cycle, is the one introduced by myself to compute the damage in the present climate. Since different ranges of years can be used to compute the expected damage CMIP based in present climate, several $v0$ variables are defined according to the preference. Such $v0$ variables are necessary to compute the statistic of the river discharges for a chosen period.

```
vnew = np.concatenate((rdis, rdisrcp), axis=0)
# Baseline 1971-1987
#v0 = rdis[0:16, xN0fake, yN0fake][(rdis[0:16, xN0fake, yN0fake] >
    Qprotection)]
# Baseline 1988-2005
#v0 = rdis[16:35, xN0fake, yN0fake][(rdis[16:35, xN0fake, yN0fake] >
    Qprotection)]
# Baseline 1990-2018
v0 = vnew[20:48, xN0fake, yN0fake][(vnew[20:46, xN0fake, yN0fake] >
    Qprotection)]
for gcm in lista:
 if gcm in model:
     yi=years[gcm][0+gwl]
     yf=years[gcm][1+gwl]
     yi0 = 35 + yi
     yf0 = 35 + yf
     e = 0
     D_base = 0
     D_NBS = 0
     for Qev in v0:
         logRP = (Qev - Fit[1]) / Fit[0]
         logRPqr = ((100 - red) / 100 * Qev - Fit[1]) / Fit[0]
         e = e + 1
         D_base = damage_rel[np.argmin((abs(Damage_x - logRP)))]
         if logRPqr > -np.log(np.log(49.88 / (49.88 - 1))):
             D_NBS = damage_rel[np.argmin((abs(Damage_x - logRPqr)))]
             out_baseline_NBS[m] = out_baseline_NBS[m] + D_NBS / 27.0
         else:
             D_NBS = 0
         out_baseline[m] = out_baseline[m] + D_base / 27.0
         reduct_baseline[:, m, e] = [logRP, logRPqr, (100 - red) / 100,
    Qev, D_base, D_NBS]
```

Listing 4.8: logical condition if

In the following listing, the expected damage for a GWL of 1.5°is computed. The logical condition if is introduced since the General Circulation Models (GCMs) forecast different years in which the temperature start to be equal to 1.5°C.

```
    if gwl==gwls['1.5']:
      if yi<0:
         print('concatenate')
         v1 = vnew[yi0:yf0,xN0fake,yN0fake][(vnew[yi0:yf0,xN0fake,
    yN0fake]>Qprotection)]
         print(v1)
      else:
         v1 = rdisrcp[yi:yf, xN0fake, yN0fake][(rdisrcp[yi:yf, xN0fake,
    yN0fake] > Qprotection)]
```

```
8           print(v1)
9       e = 0
10      D_base = 0
11      D_NBS = 0
12      for Qev in v1:
13            logRP=(Qev-Fit[1])/Fit[0]
14            logRPqr=((100-red)/100*Qev-Fit[1])/Fit[0]
15            e = e + 1
16            D_base=damage_rel[np.argmin((abs(Damage_x-logRP)))]
17            if logRPqr>-np.log(np.log(49.88/(49.88-1))):
18               D_NBS=damage_rel[np.argmin((abs(Damage_x-logRPqr)))]
19               out_1_NBS[m]=out_1_NBS[m]+D_NBS/30.0
20            else:
21                 D_NBS=0
22            out_1[m]=out_1[m]+D_base/30.0
23            reduct_1[:,m,e]=[logRP,logRPqr,(100-red)/100,Qev,D_base,
    D_NBS]
24            print(out_1)
```

Listing 4.9: Damage for GWL

The python codex used to compute the damage for GWLs of 2.0°C and 3.0°C is similar to the previous, with the difference that, respectively, $v1$ and $v2$ variables are introduced to take into account the ranges of years necessary to compute the streamflow statistics in which such GWL is reached.

Chapter 5

Results

In section 5.1 of this Chapter, the model undergoes a series of tests concerning sensibility and validation. The section 5.1.1 concerns the sensibility to the Areas of Influence implemented, while 5.1.2 concerns a river streamflow validation of the model comparing the present climate damage observed and estimated by CMIP multi-model ensemble. Then in section 5.1.3 the properties of the multi-model ensemble and flood damage are analyzed. Finally, in section 5.1.4 a validation of the damage in present climate is performed by making a comparison between the one estimated by CMIP based and the one observed EFAS based. In the last section, 5.2, an estimation of flooding risk in future climate scenarios is presented.

5.1 Model validation

To make an assessment of the sensibility and validation of the model is necessary to verify which assumptions made are the more stringent and which of them, are the major source of uncertainty. The first test concern the sensibility of the model to our assumption of Areas of Influence. The second test performs a validation of the river discharge by verifying if the multi-model ensemble estimate, for the present climate, the correct magnitude of streamflow for different return periods, by comparing the simulations with the observations. The analyses which concern the ensemble, aim to quantify and characterize the uncertainty. The first test of ensemble properties verify which model introduces most uncertainty, while the second determines if the number of the model is sufficient to make estimations. Another uncertainty that could be quantified, concerns the observed streamflow, which is not performed due to a lack of metadata of them.

5.1.1 Area of Influence assumption

In Chapter 3.4 we defined the Areas of Influence (AoI) as the assumption that the river network point, which determines the flooding height in a domain point, is the nearest one to such domain point. In this way, we can link, uniquely, which point of the river network determines the flooding height in a certain domain point during a flood event

$$p(h_i)dh_i = g(Q(r_i))dQ,$$

where r_i is the river network point, and h_i is the domain point susceptible to flooding events. To ensure that this assumption is not a sink of large uncertainty, the sensibility is evaluated with respect to the perturbation of the river point by changing the point r_i used to compute the flood damage in the point i. In Fig. 5.1 the dots represent the original river network points (the unperturbed r_i) used by the model to compute

the damage, meanwhile, the crosses represent a set of alternative river network points (perturbed i), that can be used to compute the damage in the same area.

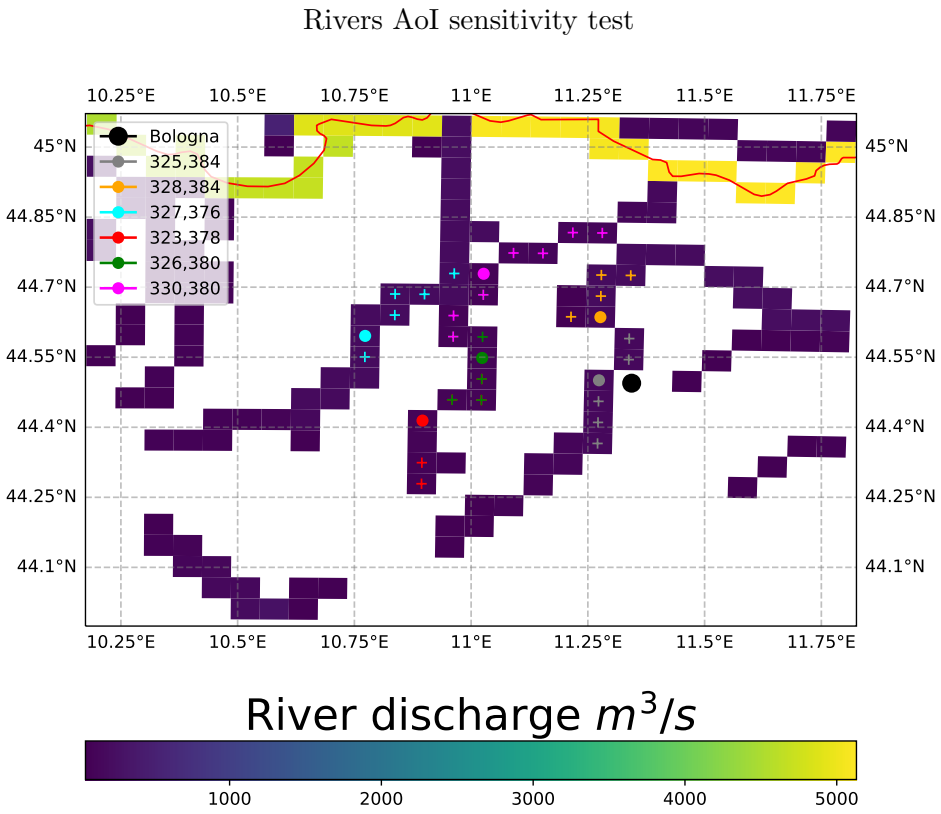

Figure 5.1: Domain points chosen, for Panaro, Reno and Secchia rivers, to perform a sensitivity test about Area of Influence (AoI).

The Fig. 5.2, 5.4, 5.3 represents the results of the AoI sensitivity test for the Panaro river in present climate and for 1.5-degree scenario. The horizontal axe values represent the river network points in ascending order distance from the original model point, which is zero, meanwhile, the vertical axe is the damage as a function of river network points.

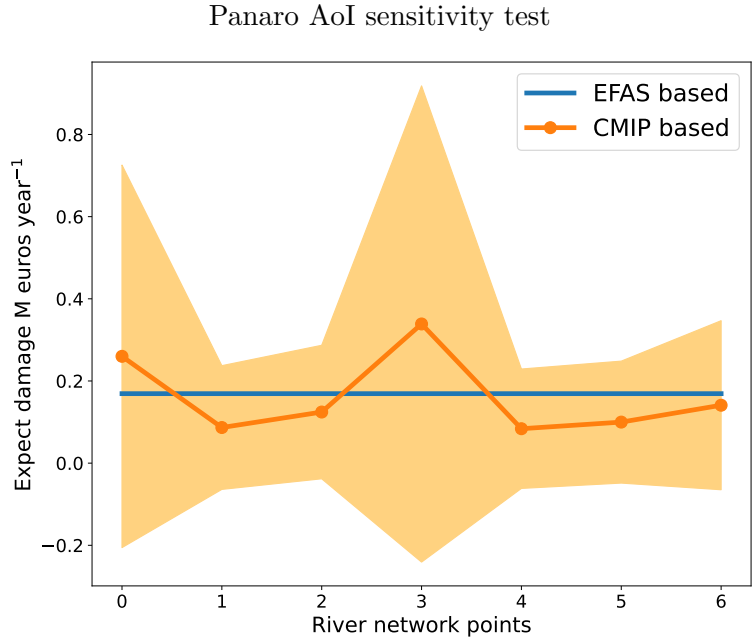

(a) Test in (323, 378) in present climate

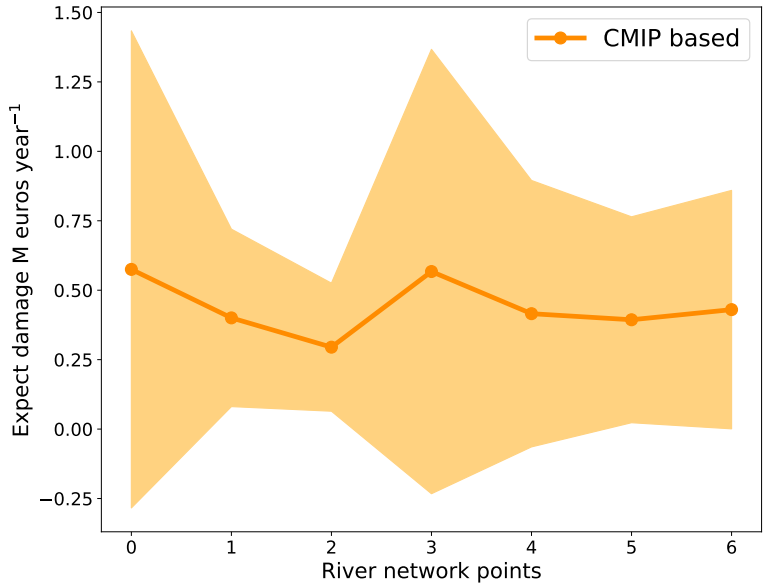

(b) Test in (323, 378) for a 1.5 Degree scenario

Figure 5.2: AoI sensitivity test accomplished for the original river network point (323, 378) of Panaro river, in which 7 nearest points are considered, in increasing distance from original, to compute the damage and to show if it depends on the points chosen; present climate and 1.5-degree scenario are considered.

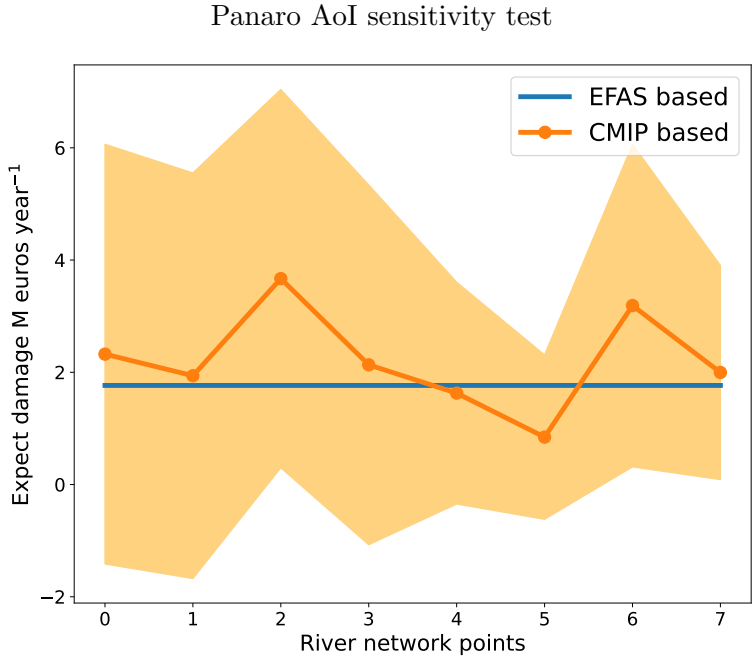

(a) Test in (326, 380) in present climate

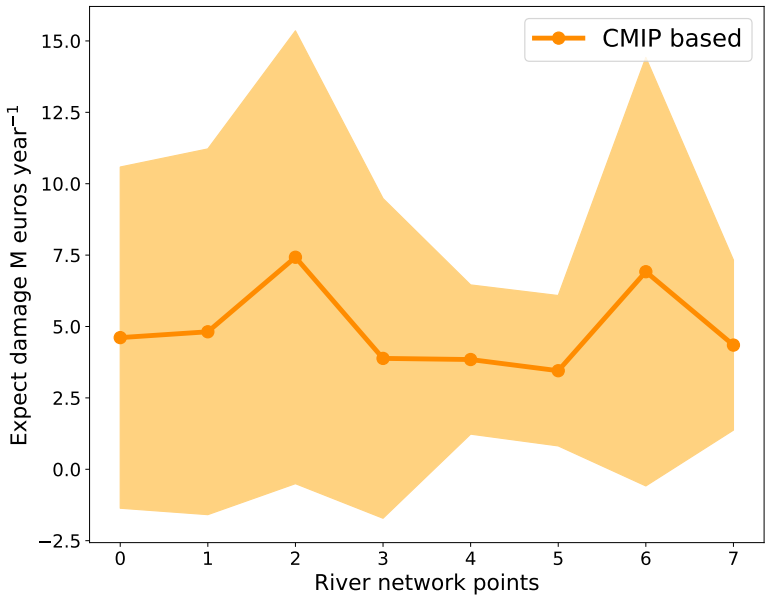

(b) Test in (326, 380) for a 1.5 Degree scenario

Figure 5.3: AoI sensitivity test accomplished for the original river network point (326, 380) of Panaro river, in which 7 nearest points are considered, in increasing distance from original, to compute the damage and to show if it depends on the points chosen; present climate and 1.5-degree scenario are considered.

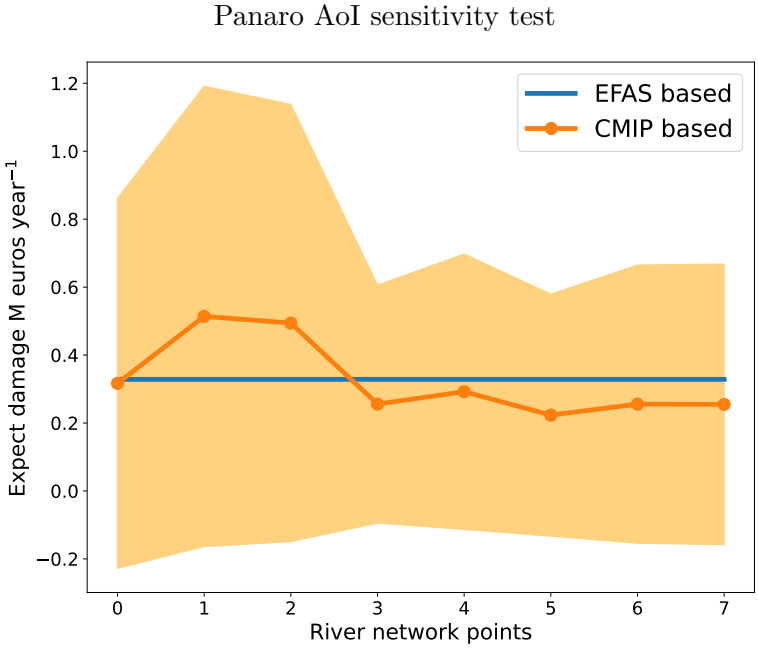

(a) Test in (330, 380) in present climate

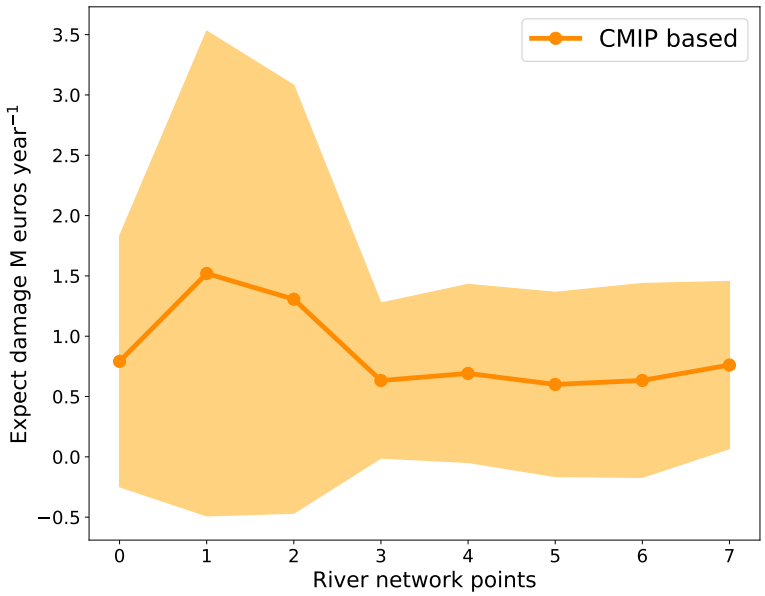

(b) Test in (330, 380) for a 1.5 Degree scenario

Figure 5.4: AoI sensitivity test accomplished for the original river network point (330, 380) of Panaro river, in which 7 nearest points are considered, in increasing distance from original, to compute the damage and to show if it depends on the points chosen; present climate and 1.5-degree scenario are considered.

In a present climate, Fig. 5.2a, 5.3a and 5.4a, the larger damages fluctuations respect to the original point are respectively 0.17, 1.47 and 0.9 M euros years^{-1} (greater amplitude of the fluctuation the greater will be ensemble spread, i.e., disagreement between models). Such values are smaller than the multi-model ensemble uncertainty that is of the order of tens of millions of euros years^{-1} (see STD in 5.1). This means a weak dependence on the river network points chosen to compute the damage. As regards the test of the 1.5-degree scenario, the results are shown in Fig. 5.2b, 5.3b and 5.4b, to determine if in a warmer earth a different sensibility could become possible. In this case,

the greatest damage fluctuations are respectively, 0.28, 1.15 and 0.19 M euros years^{-1}, which compared with multi-model ensemble uncertainty, that is of the order of tens of millions euros years^{-1} (see STD in 5.1), shown that in warmer earth does not change such sensibility. For Reno and Secchia rivers the same procedure for the Panaro river is performed.

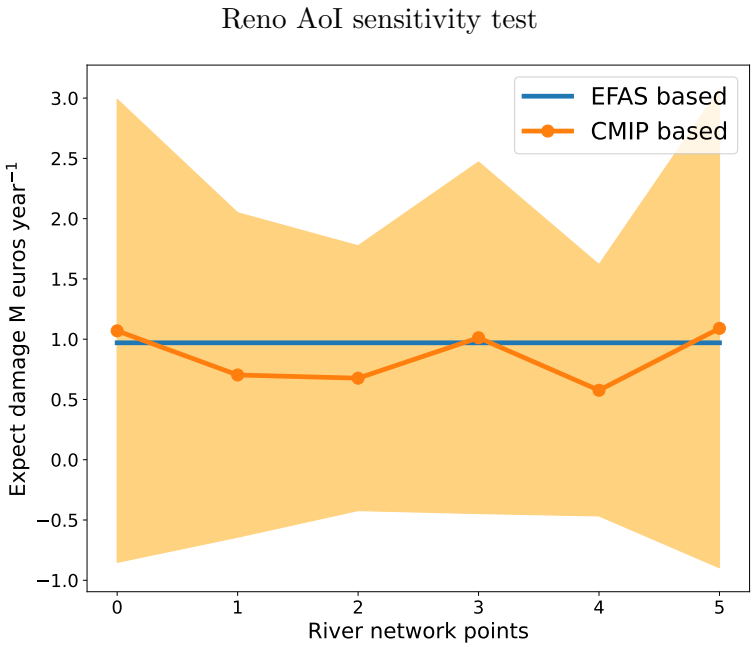

(a) Test in (325, 384) in present climate

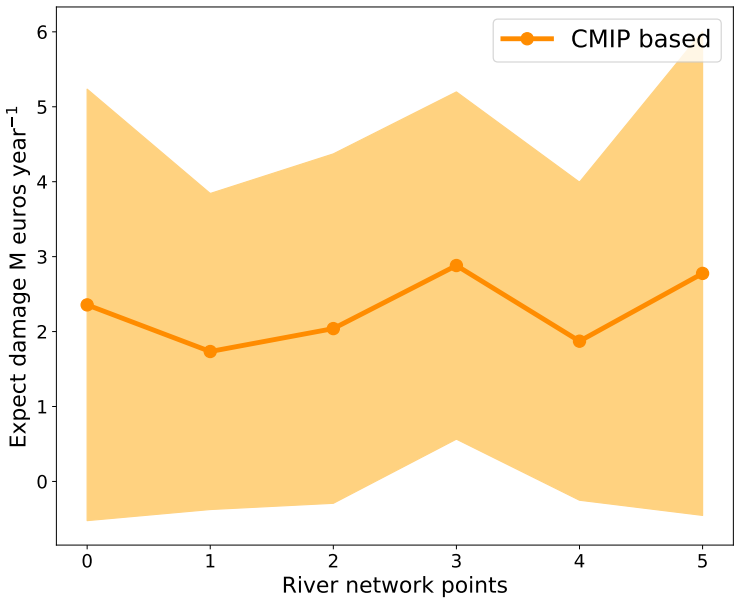

(b) Test in (325, 384) for a 1.5 Degree scenario

Figure 5.5: AoI sensitivity test accomplished for two original river network point (325, 384) of the Reno river, in which 5 points are considered, in increasing distance from original, to compute the damage and to show if it depends on the points chosen; present climate and 1.5-degree scenario are considered.

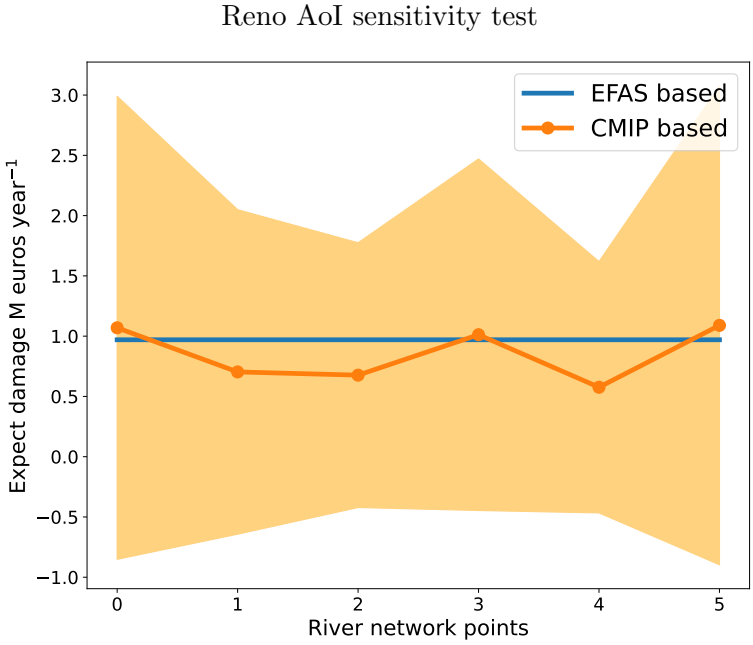

(a) Test in (328, 384) in present climate

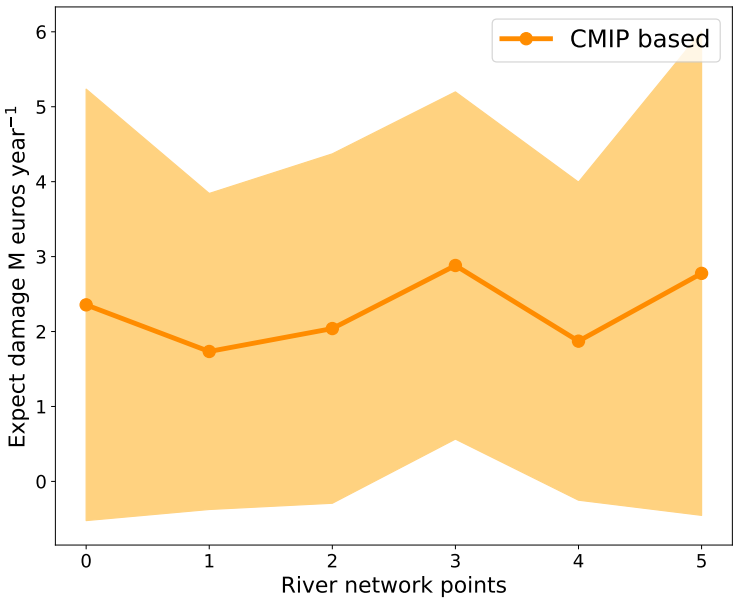

(b) Test in (328, 384) for a 1.5 Degree scenario

Figure 5.6: AoI sensitivity test accomplished for two original river network point (328, 384) of the Reno river, in which 4 points are considered, in increasing distance from original, to compute the damage and to show if it depends on the points chosen; present climate and 1.5-degree scenario are considered.

In the Reno river, for present climate, Fig. 5.5a, 5.6a and 1.5-degree scenario, Fig. 5.5b, 5.6b shown, like for the Panaro river, a weak dependence from the river network points to compute the damage, i.e. the order of the fluctuations are 0.1 million euros years$^{(}-1$), while the multi-model ensemble uncertainty is the order of tens of millions euros years$^{(}-1$) (see STD in 5.2). In the same way, as regards the Secchia river, Fig. 5.7, the fluctuations are 0.01 million euros years$^{(}-1$), while the multi-model ensemble uncertainty is the order of million euros years$^{(}-1$) (see STD in 5.3). This last results lead to the same consideration as for the other two rivers.

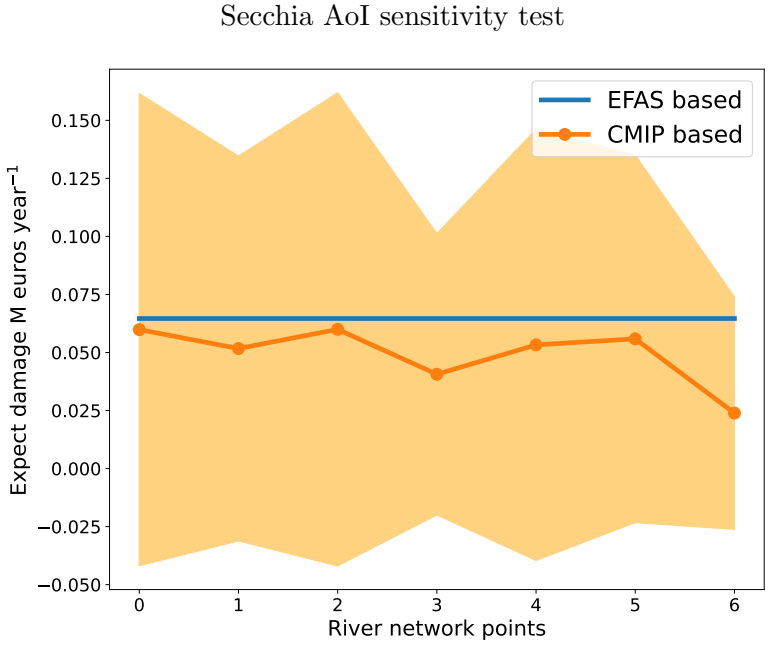

(a) Test in (327, 376) in present climate

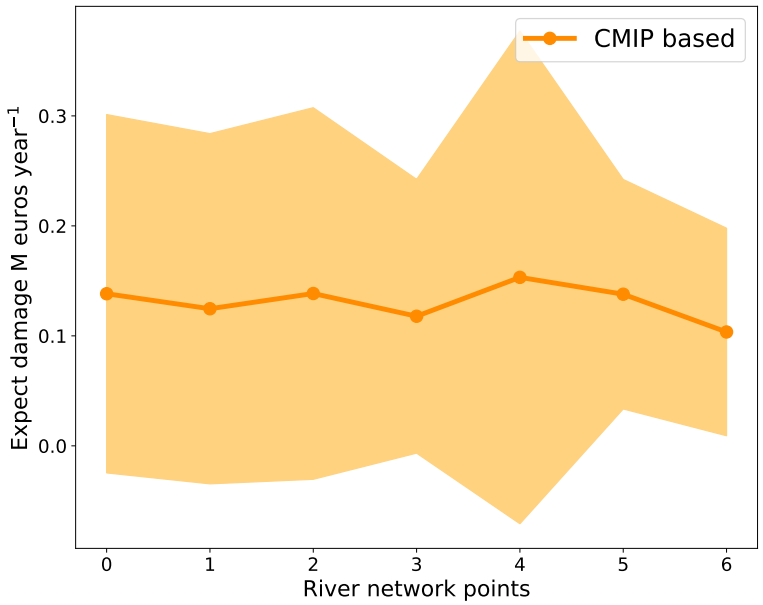

(b) Test in (327, 376) for 1.5 Degree scenario

Figure 5.7: AoI sensitivity test accomplished for the original river network point (327, 376) of Secchia river, in which 6 nearest points are considered, in increasing distance from originals, to compute the damage and to show if it depends on the points chosen; present climate and 1.5-degree scenario are considered.

In conclusion, the method proposed to compute the damage in a certain AoI fit in an appropriate way for these three rivers, which then shares the fact that the basin geometry is simple and the rivers are developed on a plane region. Probably in more complex and more slopped backgrounds, an alternative way must be used to compute which river network points determine the flooding height in an area.

5.1.2 River streamflow validation

In this model, we make the assumption that an event characterized by a flooding height H has a probability $P(H)$ to happen, and this is dependent on the return period $T(Q)$ to have a certain river discharge Q. In order for the model to be reliable, it is of relevant importance to analyze the streamflow as a function of the return period estimated by the multi-model ensemble in present climate. A comparison is done between the streamflow estimated and the one observed by station rivers. In the following figures, Fig. 5.8, 5.9, 5.10, 5.11, 5.12 and 5.13, the rivers discharge as a function of reduced variable is plotted by taking into account the multi-model ensemble and data reported in Tab. 3.3. Since its trough the coefficients of the linear regression that the model estimate the statistic of the river discharge, rather than values explored by the ensemble, the important feature to check is the slope that regression exhibits,. Therefore, the rate of growth of the simulated streamflow as a function of return period must be similar to the observed one. By referring to Fig. 5.8, the intercept observed is 423 m^3s^{-1}, while the range of intercept explored by the multi-model ensemble is 495 m^3s^{-1} (maximum value minus minimum value) with a mean value of 353 m^3s^{-1}. As regards the slope, the one observed is 196 m^3s^{-1} while the mean of the simulated slopes is 137 m^3s^{-1}. On average, we can say that the multi-model ensemble reproduces correct streamflow increasing for growing return periods.

Simulated flood frequency curves in present climate in the Panaro river

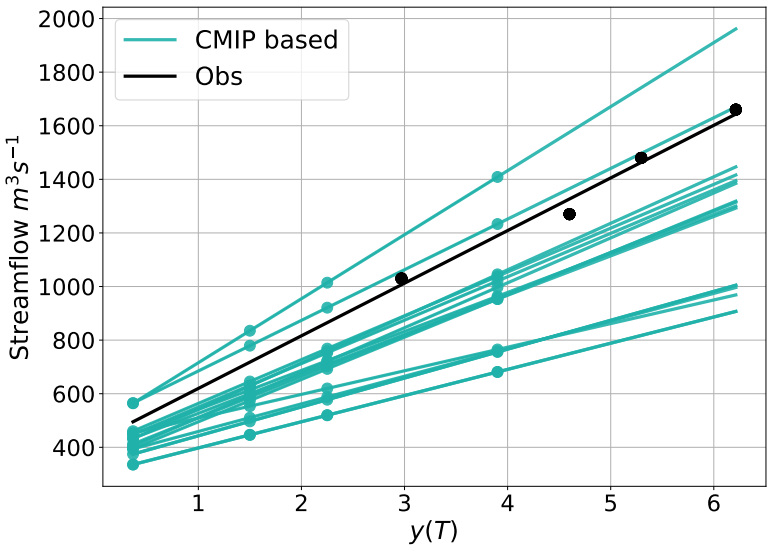

Figure 5.8: Flood frequency analysis for the Panaro river. Black dots indicate the streamflow values for 4 different return periods as provided by AIPO [24] at San Cesario sul Panaro (11.034° E 44.562° N). The black solid line is the corresponding flood frequency curve obtained by fitting a Gumbel distribution. Blue dots are the streamflow at 4 return periods obtained via C3S model chains in the same place.

By referring to the next figures, Fig. 5.9 and Fig. 5.10, the intercepts observed are respectively 256 m^3s^{-1} and 995 m^3s^{-1}, while the range of intercept explored by the multi-model ensemble is 689 m^3s^{-1} with a mean value of 492 m^3s^{-1}. The slopes observed are respectively 379 m^3s^{-1} and 280 m^3s^{-1} while the mean of the simulated slopes is 189 m^3s^{-1}.

Simulated flood frequency curves in present climate in the Reno-Casalecchio river

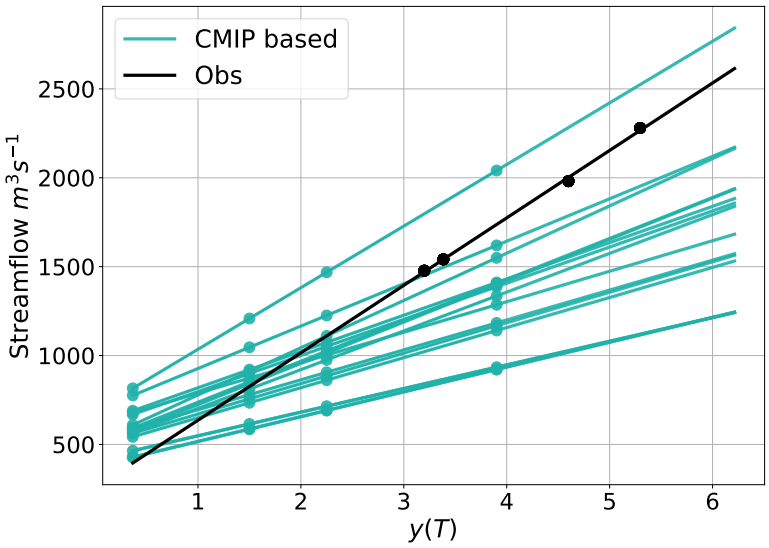

Figure 5.9: Flood frequency analysis for the Reno river. Black dots indicate the streamflow values for 4 different return periods as provided respectively by Adb Reno [26] at Casalecchio (11.280808° E 44.472343° N). The black solid line is the corresponding flood frequency curve obtained by fitting a Gumbel distribution. Blue dots are the streamflow at 4 return periods obtained via C3S model chains in the same place.

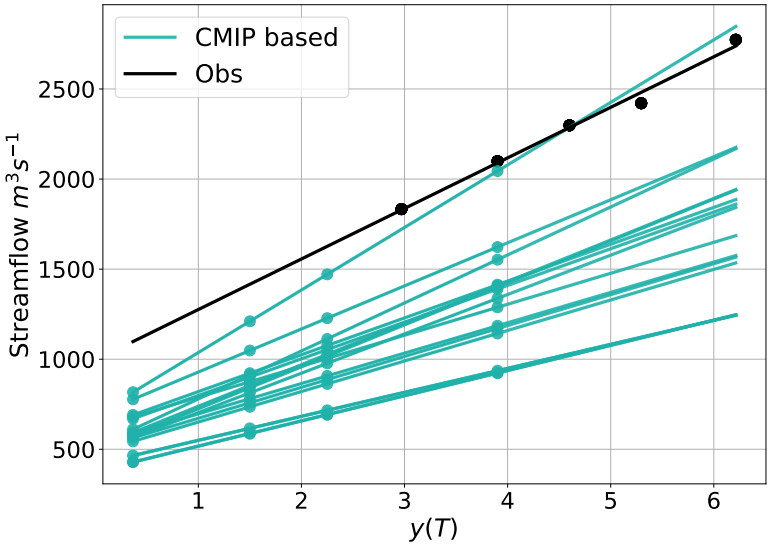

Figure 5.10: Flood frequency analysis for the Reno river. Black dots indicate the streamflow values for 5 different return periods as provided by the Comune di Marzabotto [27] at Casalecchio (11.280808° E 44.472343° N). The black solid line is the corresponding flood frequency curve obtained by fitting a Gumbel distribution. Blue dots are the streamflow at 4 return periods obtained via C3S model chains in the same place.

As concern Fig. 5.11 and Fig. 5.12, the intercept observed are respectively $235m^3s^{-1}$ and $714m^3s^{-1}$, while the range of intercept explored by the multi-model ensemble is 165 m^3s^{-1} with a mean value of 354 m^3s^{-1}. The slopes observed are respectively $253m^3s^{-1}$ and $208m^3s^{-1}$ while the mean of the simulated slopes is 149 m^3s^{-1}.

Simulated flood frequency curves in present climate in the Reno-Marzabotto river

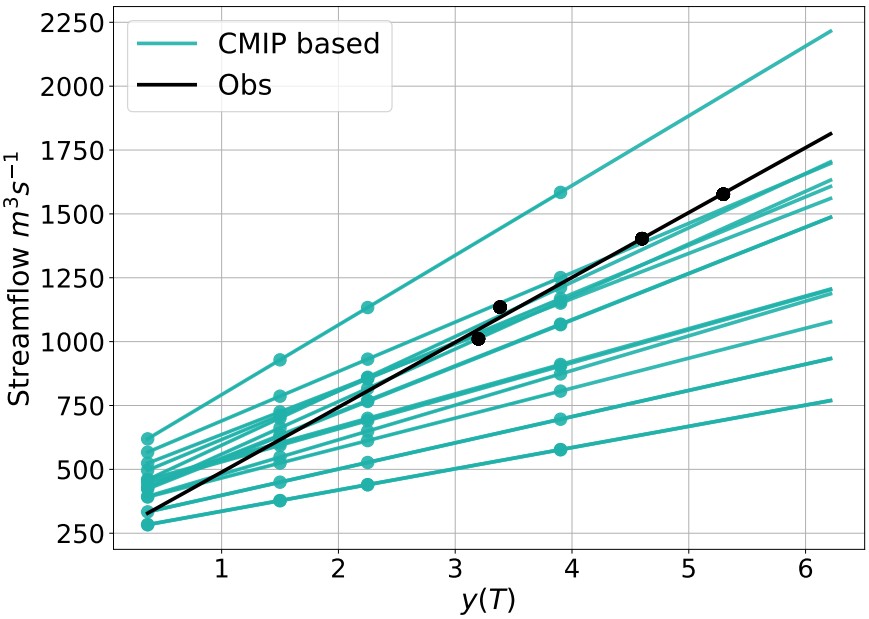

Figure 5.11: Flood frequency analysis for the Reno river. Black dots indicate the streamflow values for 4 different return periods as provided respectively by Adb Reno [26] at Marzabotto (11.208° E 44.338° N). The black solid line is the corresponding flood frequency curve obtained by fitting a Gumbel distribution. Blue dots are the streamflow at 4 return periods obtained via C3S model chains in the same place.

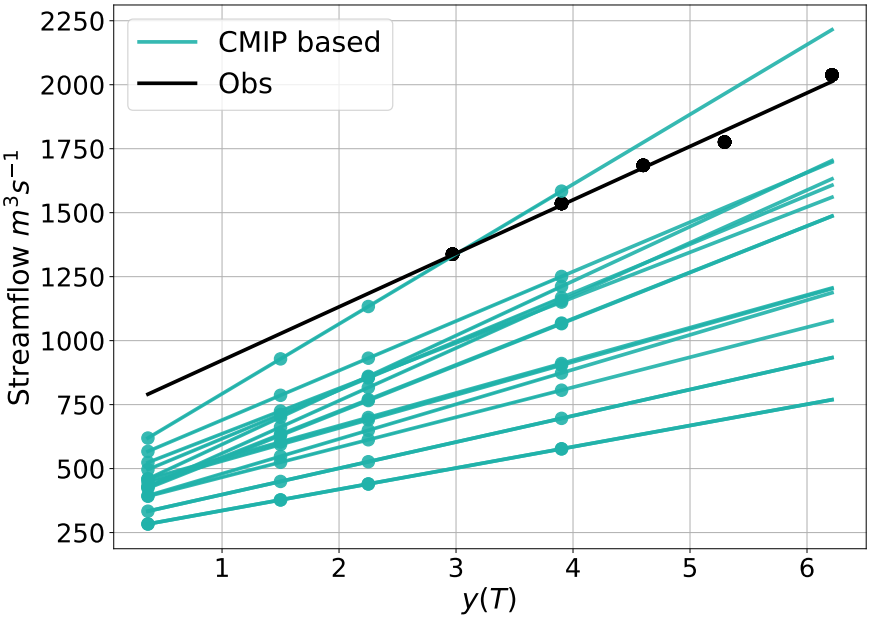

Figure 5.12: Flood frequency analysis for the Reno river. Black dots indicate the streamflow values for 5 different return periods as provided by Comune di Marzabotto [27] at Marzabotto (11.208° E 44.338° N). The black solid line is the corresponding flood frequency curve obtained by fitting a Gumbel distribution. Blue dots are the streamflow at 4 return periods obtained via C3S model chains in the same place.

Finally, by looking at Fig. 5.13, the intercept observed is 521 m^3s^{-1}, while the range of intercept explored by the multi-model ensemble is 133 m^3s^{-1} with a mean value of 545 m^3s^{-1}. As regards the slope, the one observed is 284 m^3s^{-1} while the mean of the simulated slope is 240 m^3s^{-1}. Therefore, for the Secchia river, like the Panaro, the multi-model ensemble reproduces correctly the observed slope. While for the Reno river the multi-model ensemble does not reproduce in a correct way the slope of observed data. Due to a lack of well-documented and high-quality data, e.g. concerning the observation years used, the validation for this basin is inconclusive. However such results are useful to check that model values are comparable, at least, to the order of magnitude of the observation. Since the data collection required, due to the lack of data itself, is too long, concerning the uncertainty of observed discharge we assume that it is dominated by the multi-model ensemble uncertainty.

Simulated flood frequency curves in present climate in Secchia river

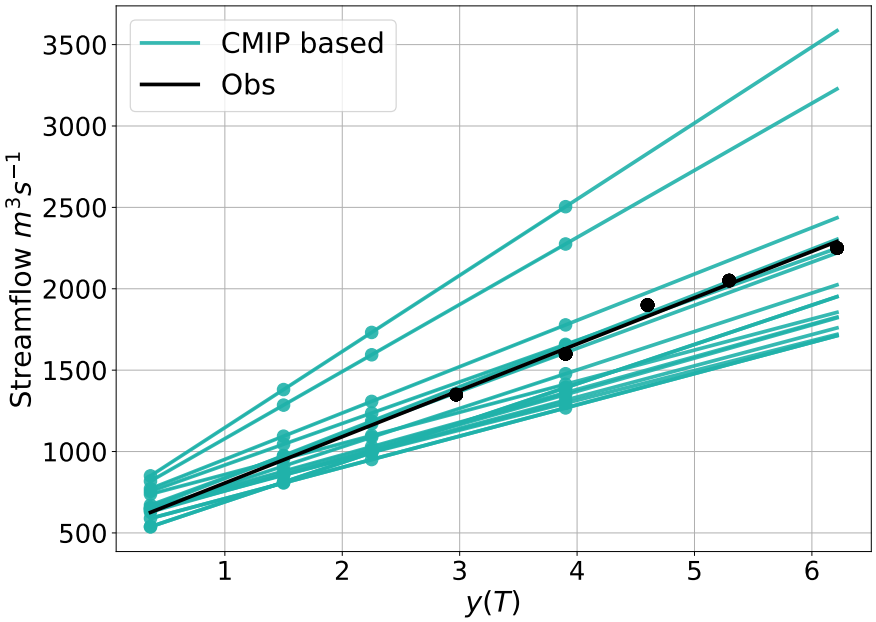

Figure 5.13: Flood frequency analysis for the Secchia river. Black dots idicate the streamflow values for 5 different return periods as provided by AIPO [25] at Concordia sulla Secchia (10.795° E 44.650° N). The black solid line is the corresponding flood frequency curve obtained by fitting a Gumbel distribution. Blue dots are the streamflow at 4 return periods obtained via C3S model chains in the same place.

5.1.3 Properties of the ensemble

This section concerns the multi-model ensemble. The first test performed is a Cross Validation (CV) test, which is a statistical technique used to assess the dependence of the results from the models of the ensemble. In this category, we found the Leave-p-out CV procedure (*Lpo*), where p denotes the number of models excluded in the computation of the test. The one performed here is the Leave One Out test ($p = 1$) in which only one model is excluded from the ensemble [29]. In our case, it consists into compute the damage, in present climate, by leaving out one of the 16 models, and repeating it for all the models. For the Panaro river, Fig. 5.14, we can see that the models which influence mostly the damage computed are: 4, 9, 10, 15, 16. Compared with the others, model 15 is the one that increases the standard deviation of the ensemble. For the Reno river, Fig. 5.15, the models that influence mostly the damage computed are 9, 10, 14, 15, and 16. Compared with the others, model 16 is the one that influences more the standard deviation of the ensemble. Finally, for the Secchia river, Fig. 5.16, the models that influence mostly the damage computed come from 8 to 16. Compared with the others, models 10 and 11 are the ones that influence more the standard deviation of the ensemble.

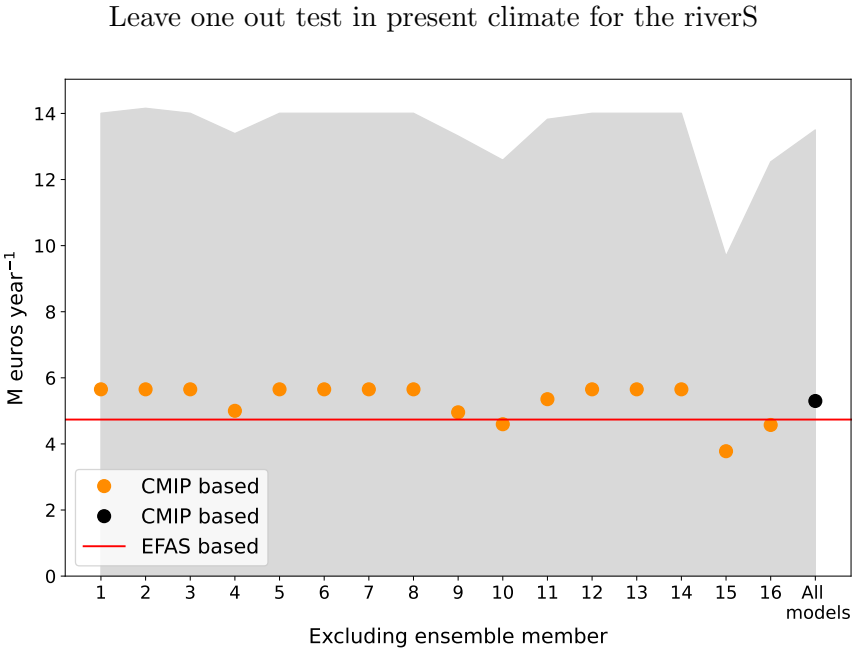

Figure 5.14: Leave one out test for the Panaro river. The vertical axe referred to the damage computed by the model, orange and black dots indicate the damage computed by the models CMIP based. The horizontal axe referred to the models excluded in the computing of the damage meanwhile the label 'All models' means that all the models are used. Orange shading is the standard deviation of the CMIP-based ensemble and the horizontal red line is the EFAS-based damage.

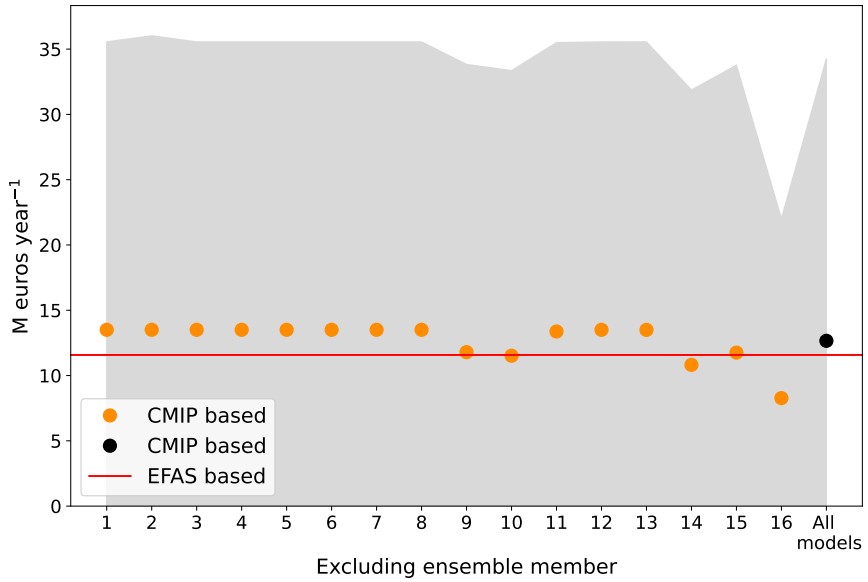

Figure 5.15: Leave one out test for the Reno river. The vertical axe referred to the damage computed by the model, orange and black dots indicate the damage computed by the models CMIP based. The horizontal axe referred to the models excluded in the computing of the damage meanwhile the label 'All models' means that all the models are used. Orange shading is the standard deviation of the CMIP-based ensemble and the horizontal red line is the EFAS-based damage.

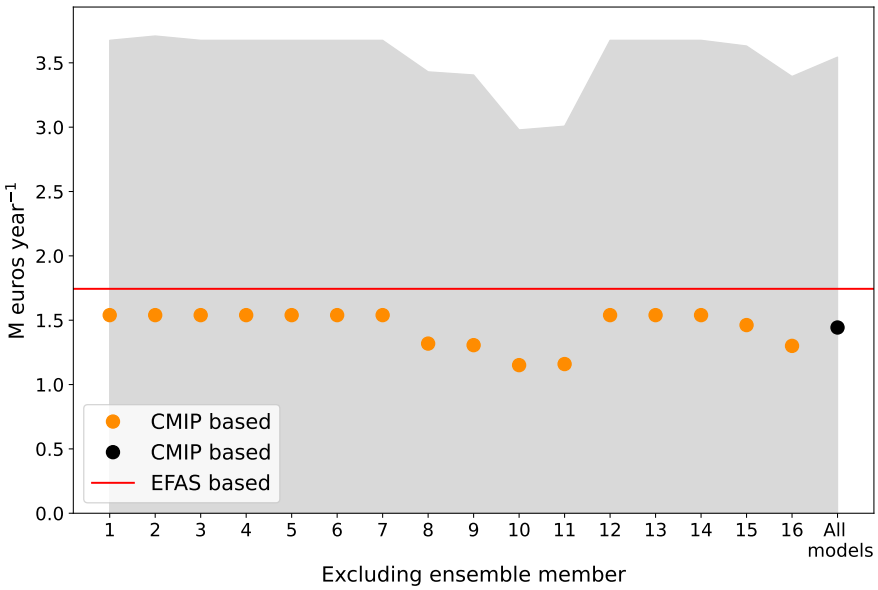

Figure 5.16: Leave one out test for the Secchia river. The vertical axe referred to the damage computed by the model, orange and black dots indicate the damage computed by the models CMIP based. The horizontal axe referred to the models excluded in the computing of the damage meanwhile the label 'All models' means that all the models are used. Orange shading is the standard deviation of the CMIP-based ensemble and the horizontal red line is the EFAS-based damage.

The second test concerning the ensemble is about the size and try to show if the number of models considered is sufficient. The rationale is to start by considering an ensemble composed of 2 models, chosen randomly, and considering all the possible com-

binations; this procedure is repeated by increasing the ensemble size until all 16 models are considered. Thereby we will have 120 ensembles composed of 2 members, 560 by 3, 1820 by 4 etc. The test aims to very if the estimated standard deviation saturates with members number N for $N \approx 16$, in that case, no more members are needed. The next figures show the standard deviation in function of ensemble size, for all the rivers, Panaro 5.17, Reno 5.18 and Secchia 5.19. By increasing the ensemble size, we have a considerable diminishing of standard deviation, this leads to conclude that the number of models CMIP based used is sufficient and no more are needed.

Ensemble size test for the rivers in present climate

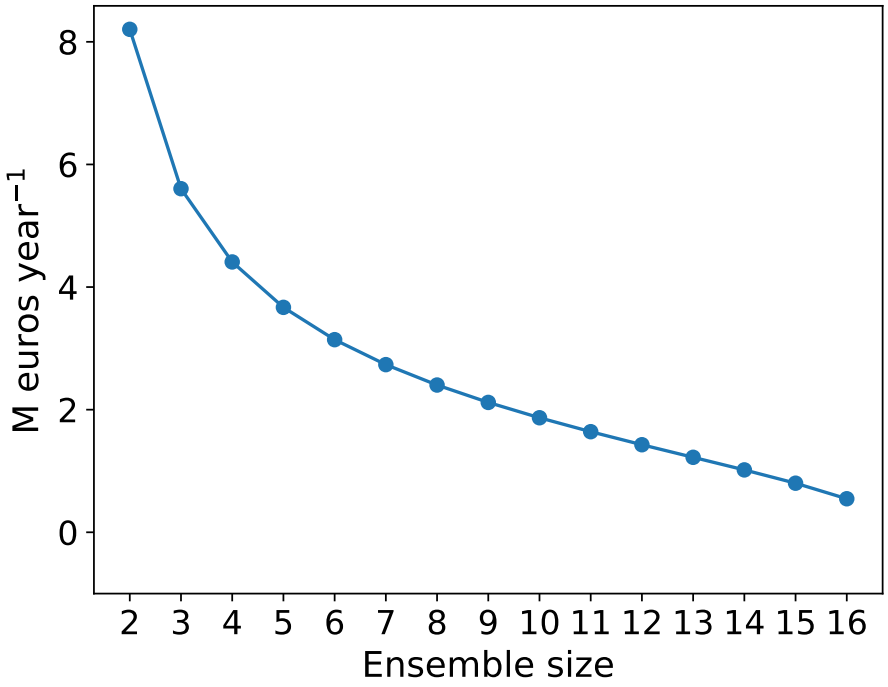

Figure 5.17: Standard deviation in function of ensemble size for the Panaro river. The vertical axe referred to the damage computed by the model, blue dots indicate the damage compute by the muti-model ensemble CMIP based. The horizontal axe referred to the ensemble size.

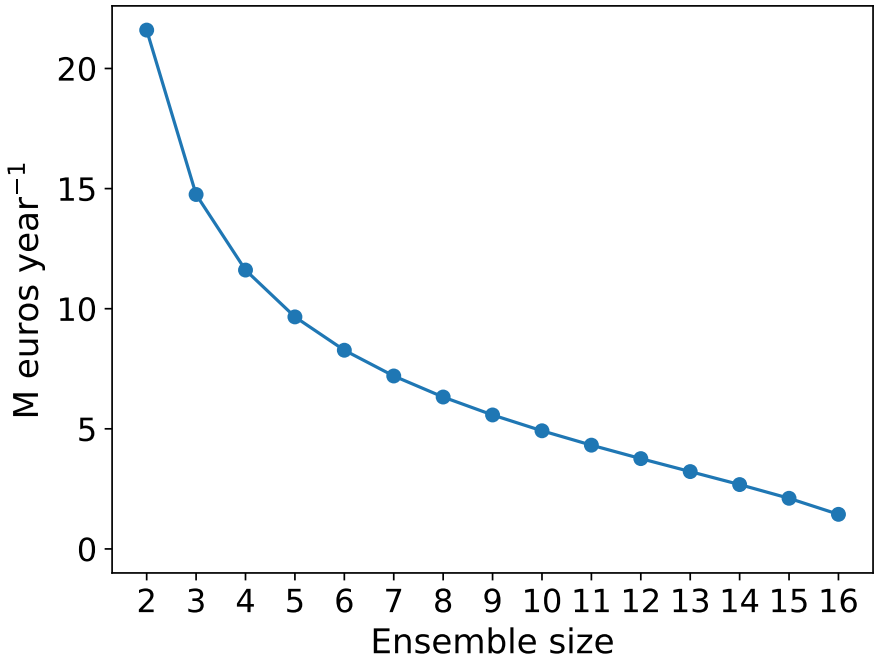

Figure 5.18: Standard deviation in function of ensemble size for the Reno river. The vertical axe referred to the damage computed by the model, blue dots indicate the damage compute by the muti-model ensemble CMIP based. The horizontal axe referred to the ensemble size.

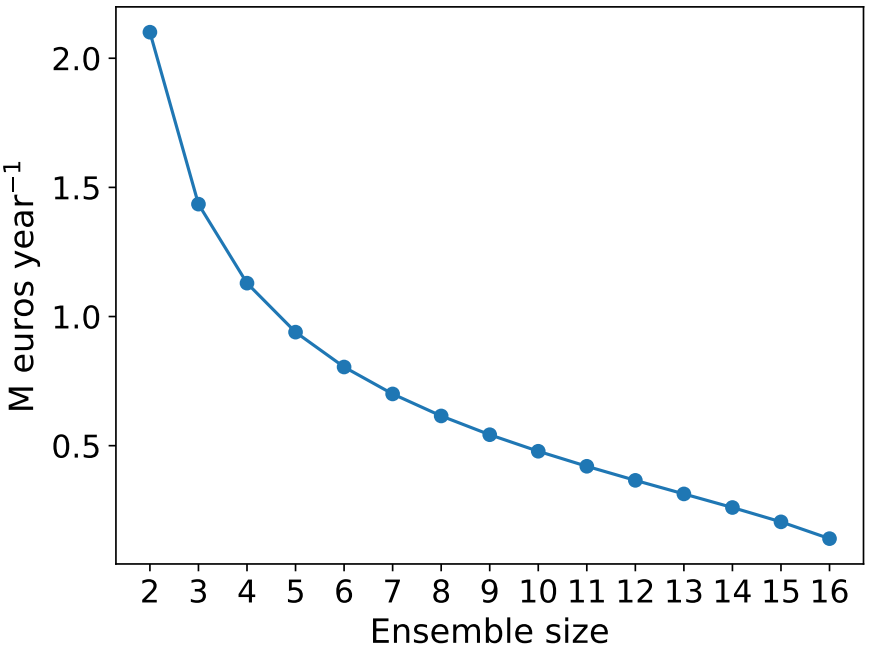

Figure 5.19: Standard deviation in function of ensemble size for the Secchia river. The vertical axe referred to the damage computed by the model, blue dots indicate the damage compute by the muti-model ensemble CMIP based. The horizontal axe referred to the ensemble size.

5.1.4 Flood damage validation

At first, a comparison between CMIP based damage in present climate (baseline), computed by using different ranges of years, and EFAS based baseline is performed to choose the correct years to use to make a correct flood damage validation in present climate. By looking at Fig. 5.20, 5.21 and 5.22 we notice that, by using (1975-2005) as years interval to define the baseline CMIP based, we overestimate the damage, due especially for the (1971-1987) contribution. Even if both (1988-2005) and (1990-2018) years ranges lead to a correct estimate of damage CMIP based compared with EFAS, since the (1990-2018) years range is used to perform the baseline EFAS based, from consistency the last range of years will be used from now to compute the CMIP baseline.

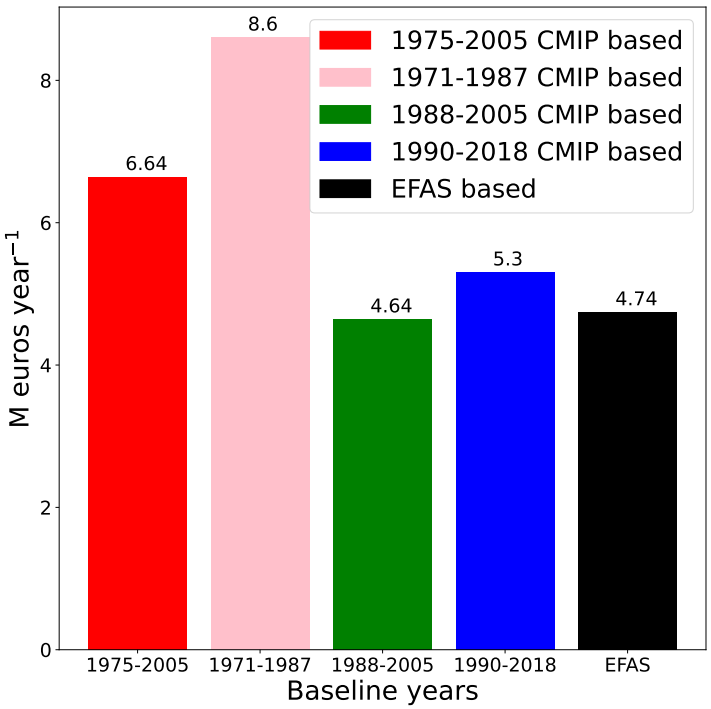

(a) Panaro river

Figure 5.20: Expected damage (baseline) for different ranges of years for the Panaro river.

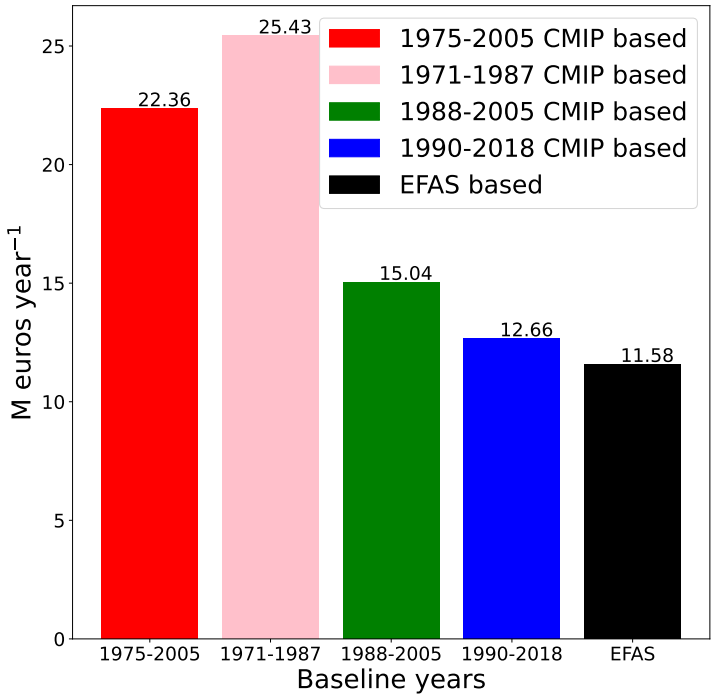

Figure 5.21: Expected damage (baseline) for different ranges of years for the Reno river.

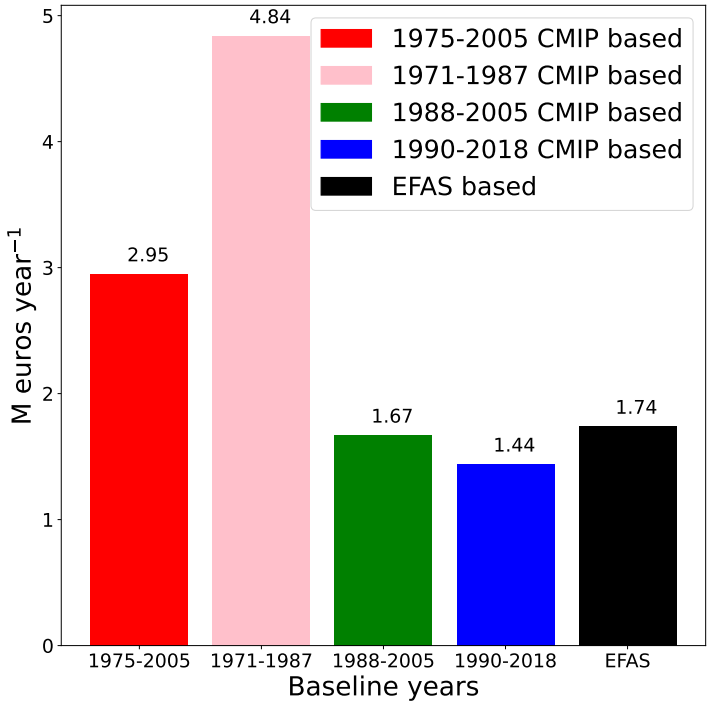

Figure 5.22: Expected damage (baseline) for different ranges of years for the Secchia river.

In the next figures, Fig.5.23, 5.24 and 5.25, for each basin and model, the expected damage CMIP based and EFAS based in present climate are shown.

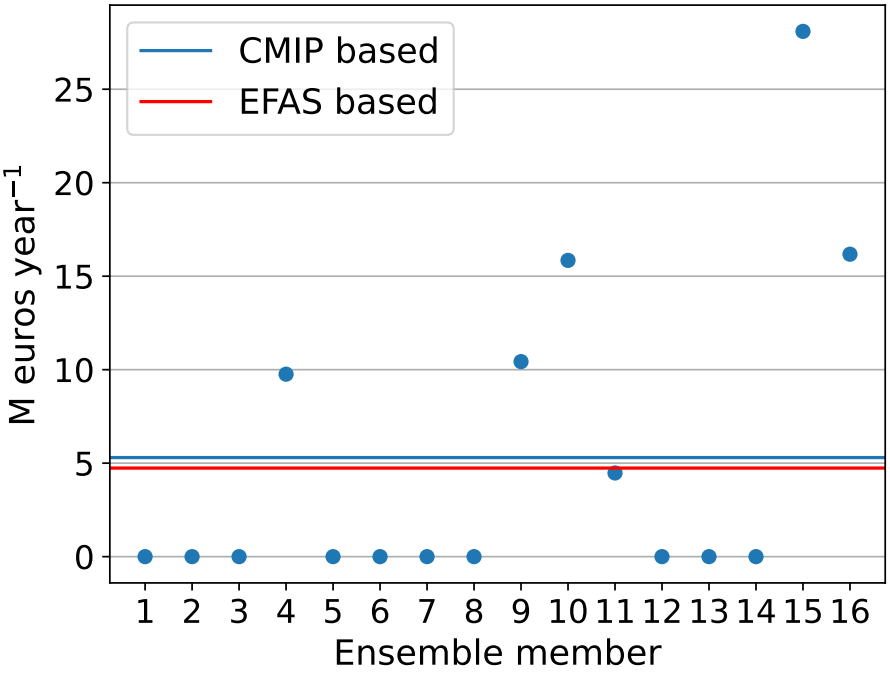

Figure 5.23: Expected damage for the Panaro river, CMIP based compared with EFAS based, relative error computed is 11%. The explicit expression of relative error is reported in Appendix B.

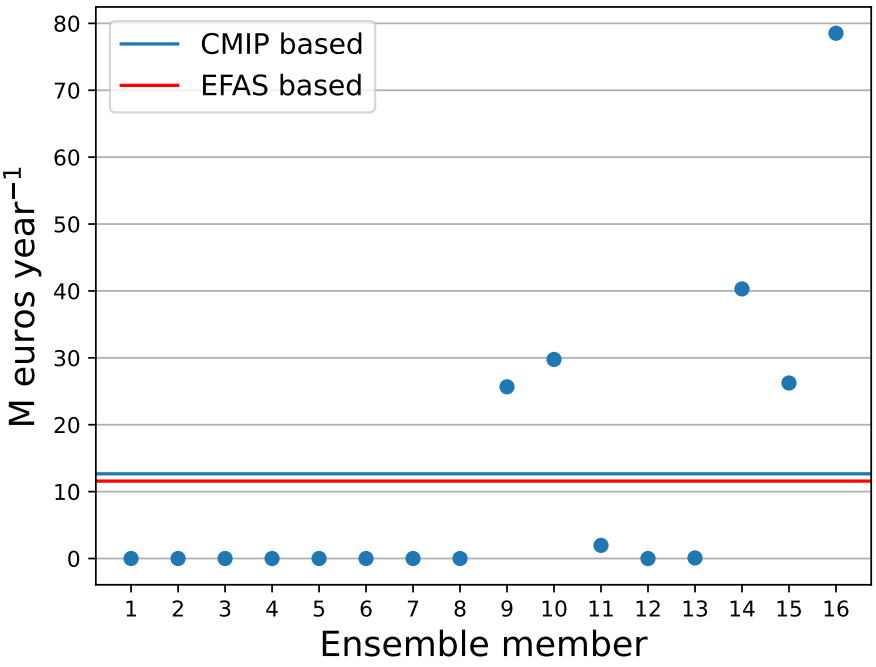

Figure 5.24: Expected damage for the Reno river, CMIP based compared with EFAS based, relative error computed is 9%. The explicit expression of relative error is reported in Appendix B.

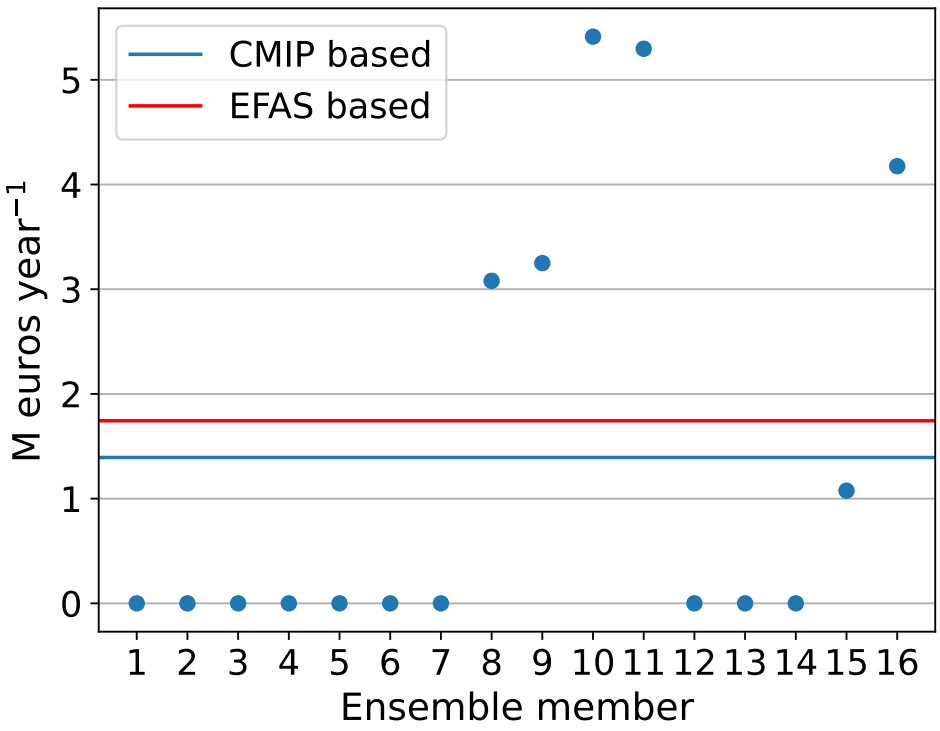

Figure 5.25: Expected damage for the Secchia river, CMIP based compared with EFAS based, relative error computed is 20%. The explicit expression of relative error is reported in Appendix B.

For all the basins, we have a good damage estimation by CMIP models, with a relative error of the order of ten percentage points. These results show good behaviour, of the model, for damage estimation in present climate, and this gives us confidence about correct estimation in future climate scenarios as well.

As shown in Fig. 5.26, 5.27 and 5.28, in each domain point and for all the basins, the mean damage of the model CMIP based is computed and then compared with one EFAS based. Fig. 5.26a shows that the domain points 3, 4, 7, 8, and 16 are the ones in which the damages are more overestimated by the model. By looking at standard deviations in Fig. 5.26b, we can deduce that members of the ensemble, in such points, disagree with each other. Fig. 5.27a shows that the domain points 4, 23, 29, 34, 46 and 51 are the ones in which the damages are more overestimated by the model. By looking at standard deviations in Fig. 5.27b, we can deduce that members of the ensemble, in such points, disagree with each other. Fig. 5.28a shows that the domain points 22, 23, 28, 29, and 48 are the ones in which the damages are underestimated by the model. By looking at standard deviations in Fig. 5.28b, we can deduce that members of the ensemble, in such points, disagree with each other.

Flood damage Panaro basin

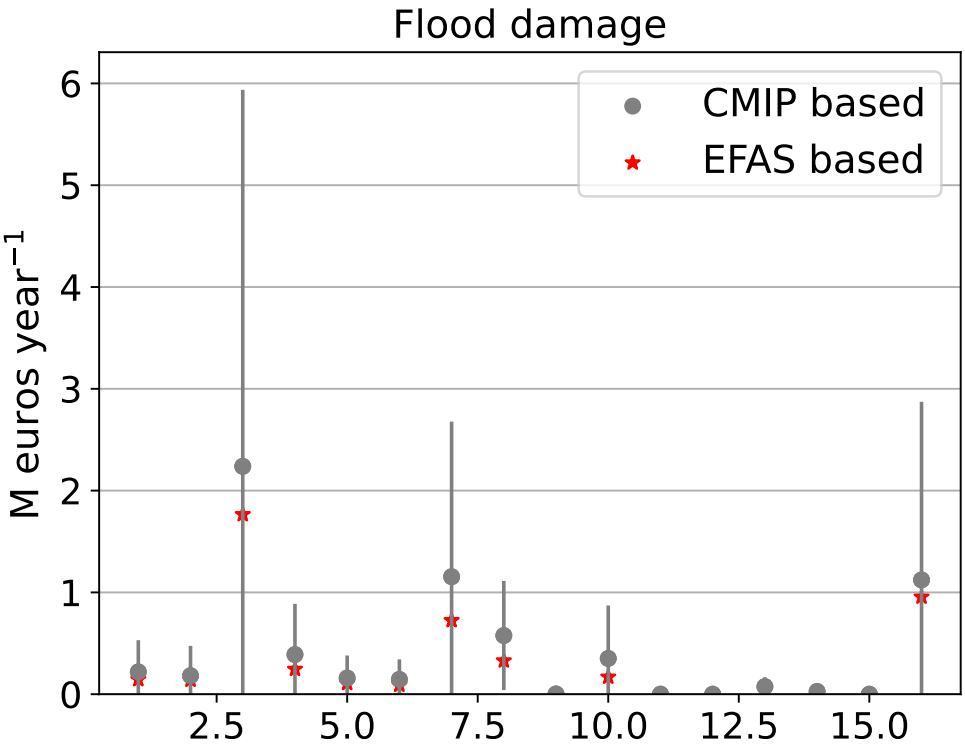

(a) Flood damage

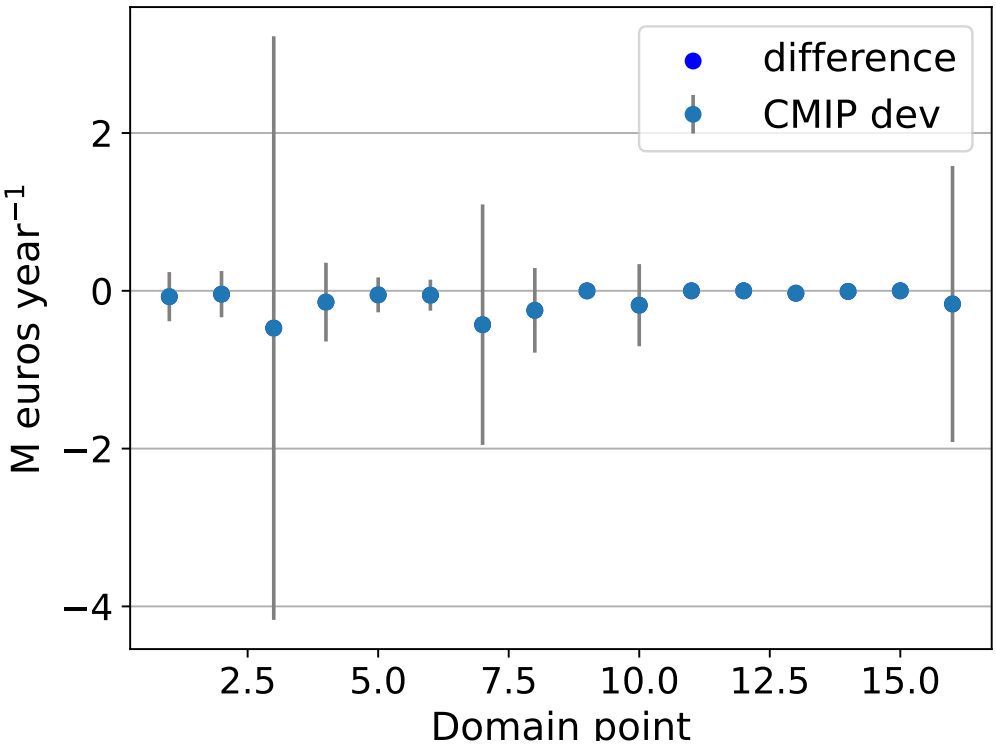

(b) Flood damage difference

Figure 5.26: Expected damage for CMIP model-based and EFAS ones (a) and the difference between CMIP and EFAS (b) in each domain point of Panaro basin.

Flood damage Reno basin

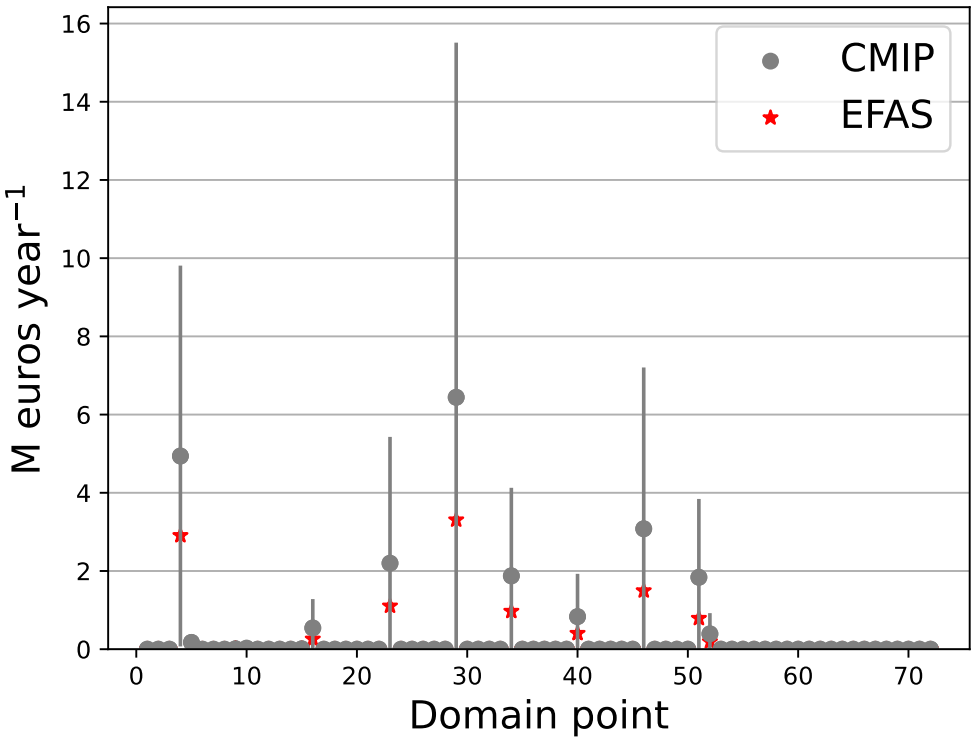

(a) Flood damage, CMIP and EFAS based, in Secchia basin

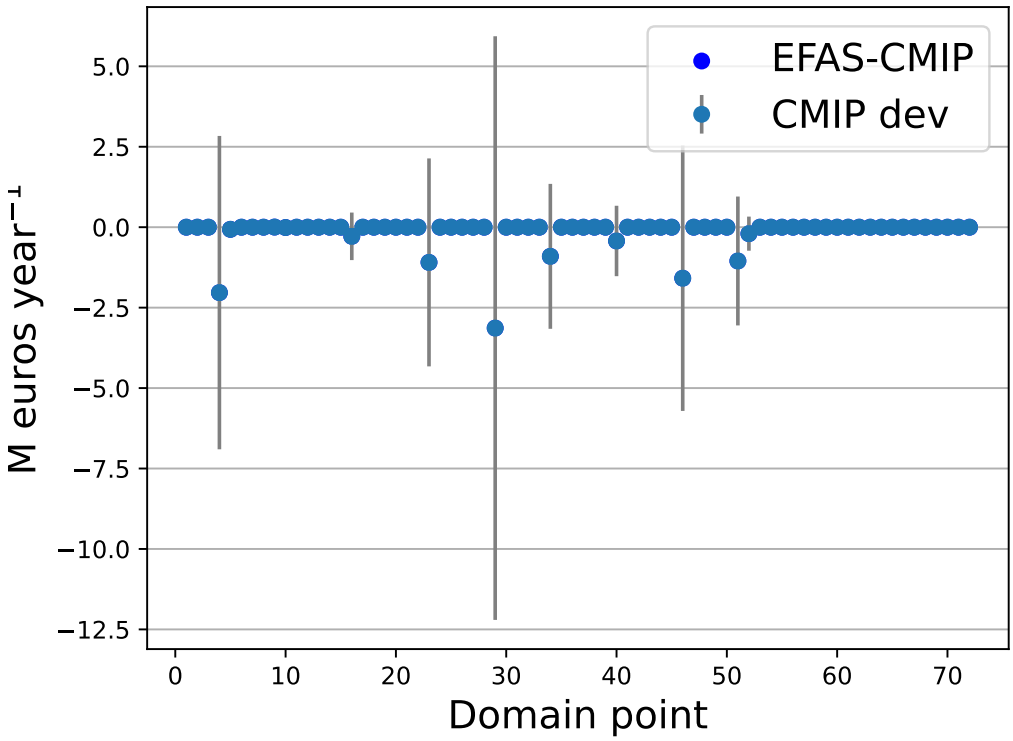

(b) Flood damage difference, CMIP and EFAS based, in Reno basin

Figure 5.27: Expected damage for CMIP model-based and EFAS ones (a) and the difference between CMIP and EFAS (b) in each domain point of Reno basin.

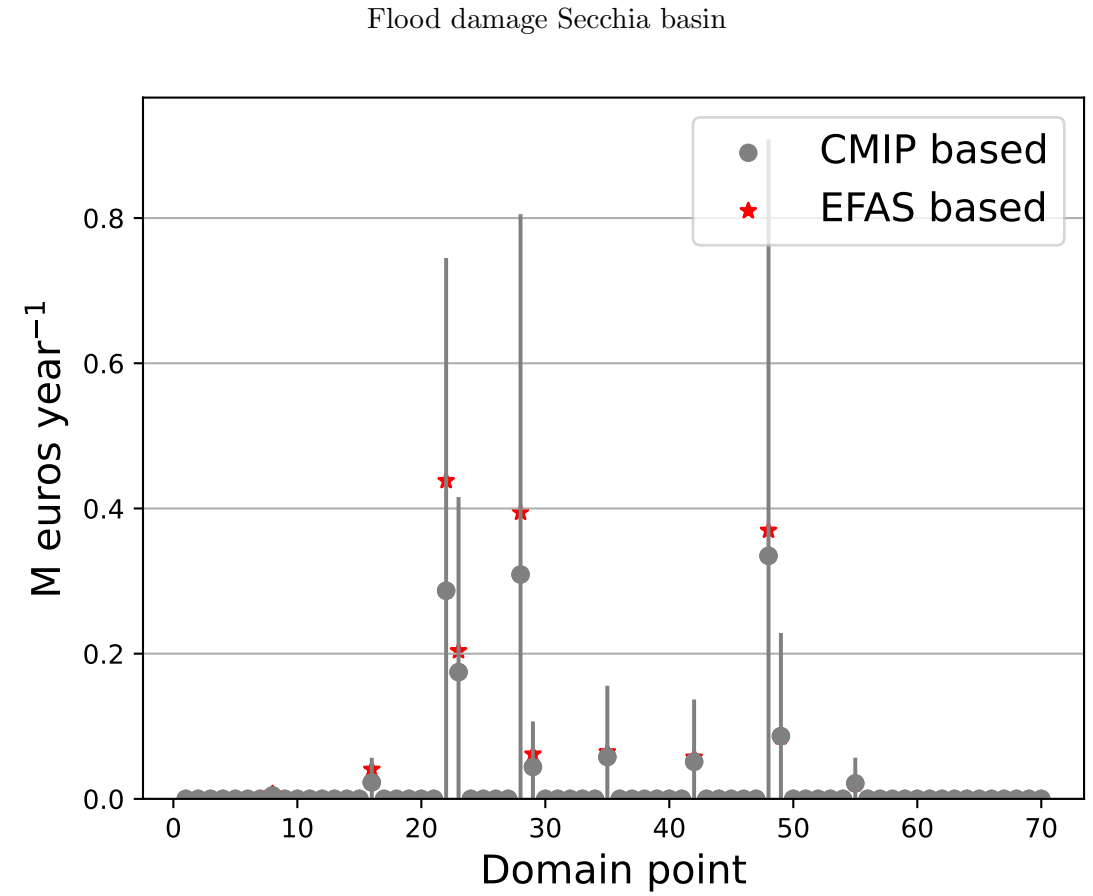

(a) Flood damage, CMIP and EFAS based, in Secchia basin

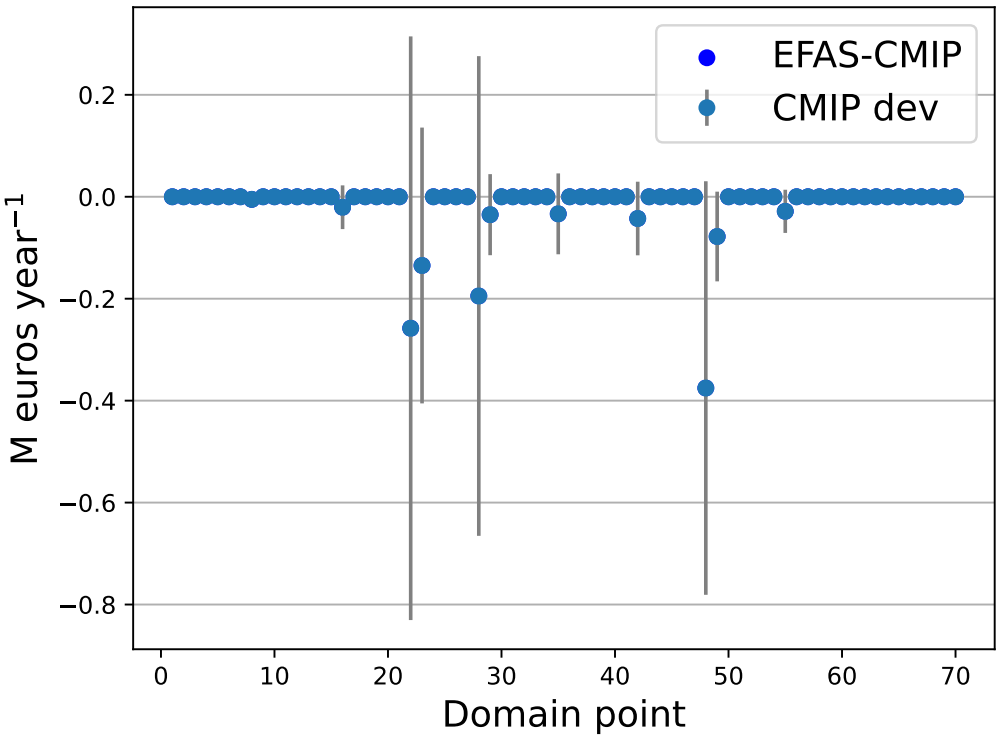

(b) Flood damage difference, CMIP and EFAS based, in Secchia basin

Figure 5.28: Expected damage for CMIP model-based and EFAS ones (a) and the difference between CMIP and EFAS (b) in each domain point of Secchia basin.

5.2 Estimating risk in future climate

Since the model takes into account a chain of models CMIP based, a projection of river discharge in future climate scenarios, until 3 degrees above pre-industrial conditions (1861-1890), can be considered. Since we assume that the statistic of flooding height is referable to the river discharge one, from river discharge projections we can obtain the flooding height ones, this means that an estimate of damage cost in the future scenarios can be done through the flood damage functions defined in 4. To show the damage cost increasing for the different degree scenario, in the next figures, Fig. 5.29, 5.30 and 5.31, box plots are performed for all the basins.

Damage cost for the Panaro river for present climate, 1.5, 2 and 3 degree scenario

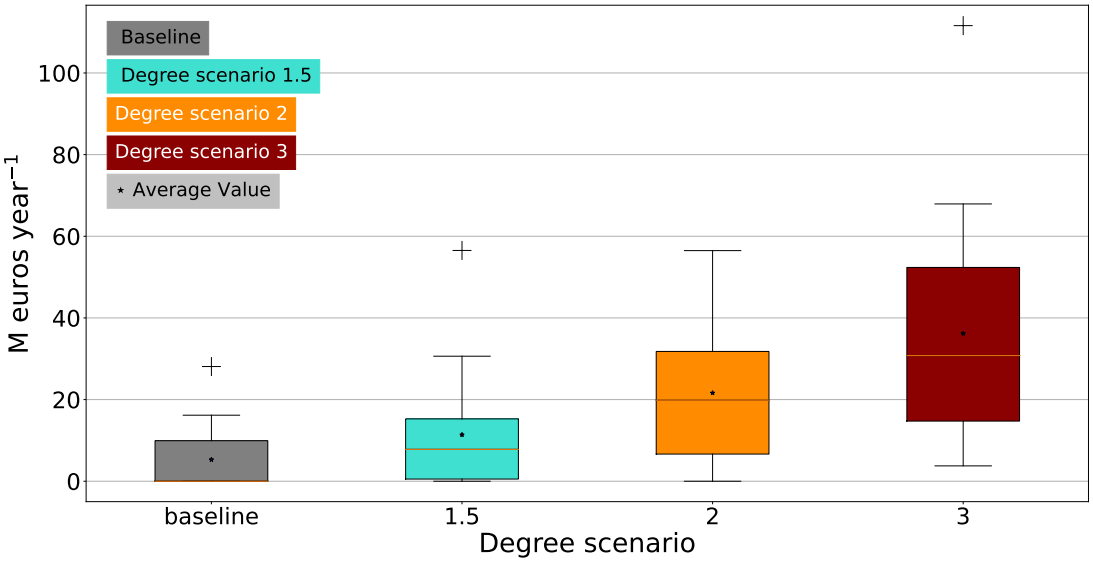

Figure 5.29: Box plots of the damage in terms of M euros years^{-1} for the Panaro river for the baseline and global warming levels of 1.5, 2.0 and 3.0 degrees.

Damage cost for the Reno river for present climate, 1.5, 2 and 3 degree scenario

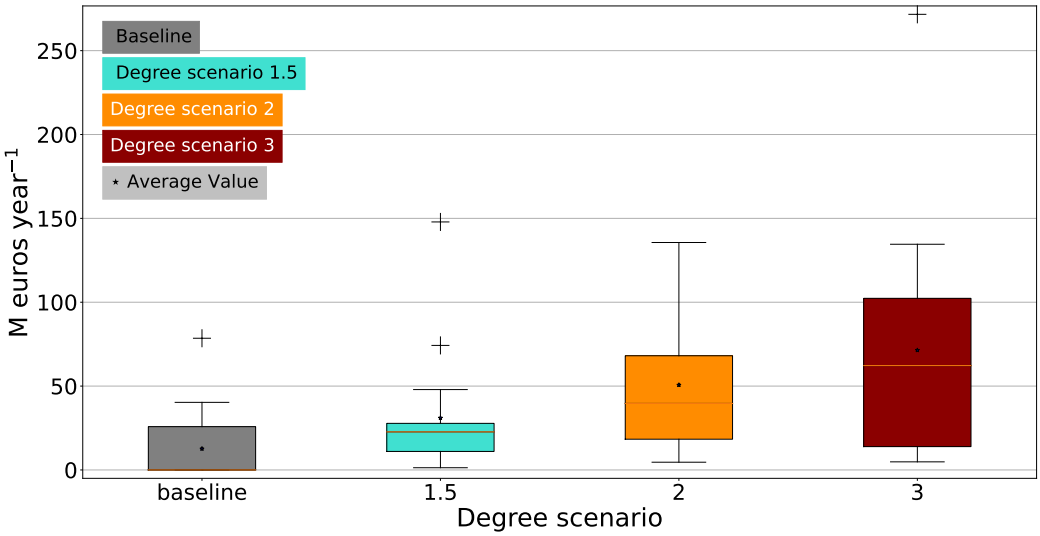

Figure 5.30: Box plots of the damage in terms of M euros years^{-1} for the Reno river for the baseline and global warming levels of 1.5, 2.0 and 3.0 degrees.

Damage cost for the Secchia river for present climate, 1.5, 2 and 3 degree scenario

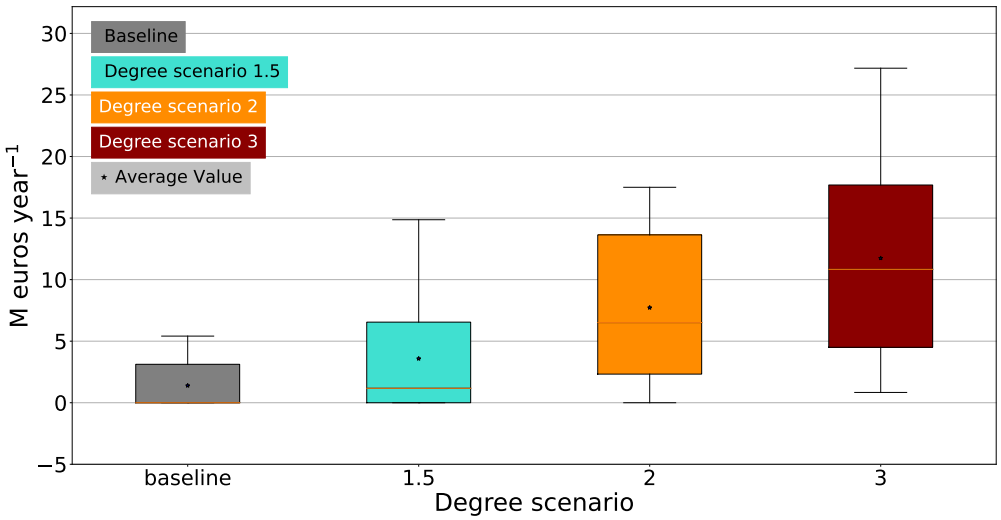

Figure 5.31: Box plots of the damage in terms of M euros years^{-1} for the Secchia river for the baseline and global warming levels of 1.5, 2.0 and 3.0 degrees.

To visualize better the shape and skewness of the distributions, the probability density functions are plotted for all the basins, Fig.5.32, 5.33 and 5.34 their respective statistic indexes are reported in Tab. 5.1, 5.2 and 5.3. By looking at the tables, for all the rivers and in all the degree scenarios, the distributions are positively skewed with a mean greater than the median, this means that the tails' distribution is right-skewed. For Secchia river, Fig. 5.34, the skewness approaches zero, so the distribution is near to symmetric. As shown qualitatively by the boxplot whiskers, for all the rivers the standard deviation and mean increase as the temperature of the degree scenario increase.

Probability density function of Damage cost for the Panaro river

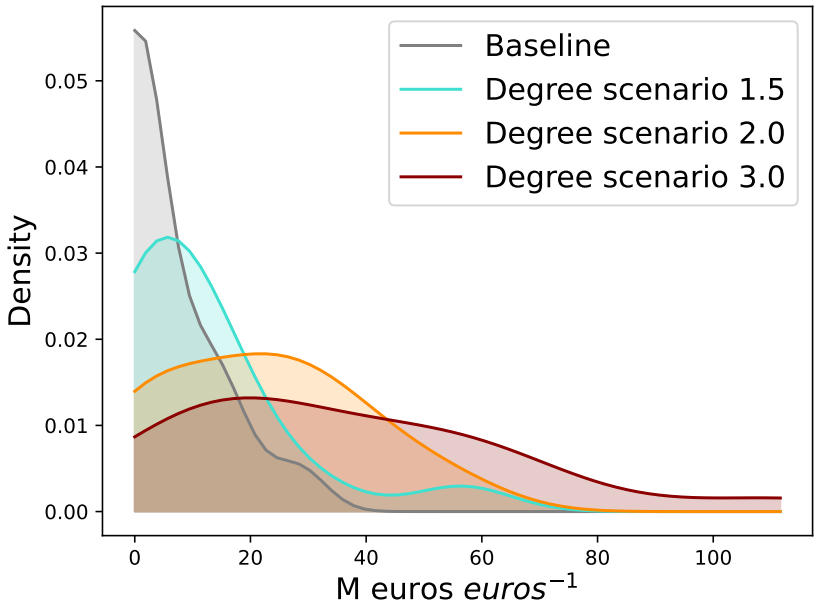

Figure 5.32: Probability density function (PDF) of damage in terms of M euros years^{-1} for Panaro in present climate and for increasing GWLs. The PDF, which is an approximation of the underlying histograms, is performed by using a Kernel density estimation (KDE) which smooths the discrete data with a Gaussian kernel, producing a continuous density estimate by using 60 bins.

Probability density function of Damage cost for the Reno river

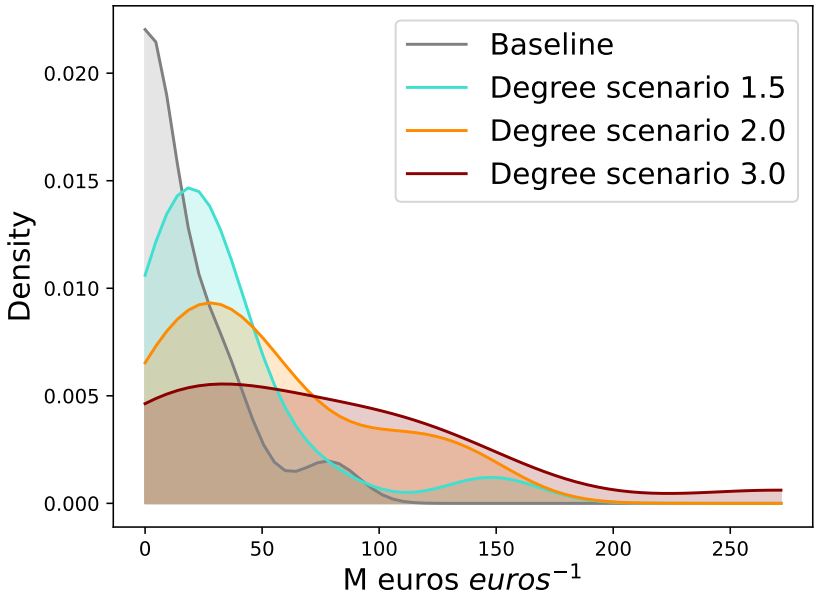

Figure 5.33: Probability density function (PDF) of damage in terms of M euros years^{-1} for Reno in present climate and for increasing GWLs. The PDF, which is an approximation of the underlying histograms, is performed by using a Kernel density estimation (KDE) which smooths the discrete data with a Gaussian kernel, producing a continuous density estimate by using 60 bins.

Probability density function of Damage cost for the Secchia river

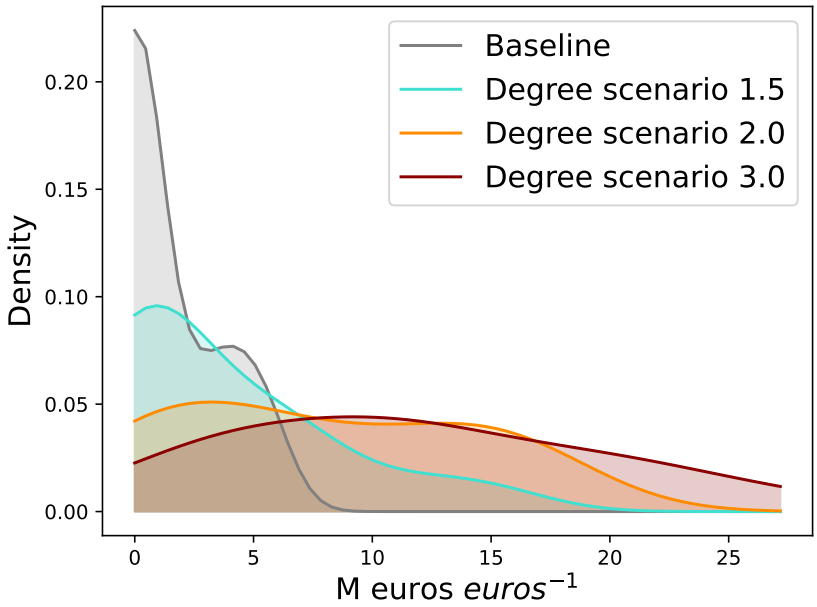

Figure 5.34: Probability density function (PDF) of damage in terms of M euros years^{-1} for Secchia in present climate and for increasing GWLs. The PDF, which is an approximation of the underlying histograms, is performed by using a Kernel density estimation (KDE) which smooths the discrete data with a Gaussian kernel, producing a continuous density estimate by using 60 bins.

Another important index computed is kurtosis, which describes the flatness of the distributions, and is a sort of measure of the distribution tails thickness, but it could be seen as a departure measure from the normal distribution. Even if the kurtosis index makes sense only for monomodal distribution, by looking at the value in Tab. 5.1, for baseline and 1.5 degrees scenario the distribution is called leptokurtic so is more pointed than the normal distribution. For 2.0 degree scenario, the index is negative, is called platykurtic, and is flatter than the normal one; for a 3.0 degree scenario the index is slightly positive and is leptokurtic but near to mesokurtic, so is flat like a normal distribution.

Table with statistic indexes relative to Panaro PDF

Degree scenario	Mean	Median	STD	Skewness	Kurtosis	SNR
Baseline	5.29	0.0	8.20	1.47	1.21	0.64
1.5	11.39	7.8	14.33	1.93	3.47	0.79
2	21.62	19.85	16.89	0.31	-0.82	1.28
3	36.19	30.76	27.94	1.07	0.79	1.29

Table 5.1: Statistic indices relative to the PDF of the Panaro river 5.32. The explicit form of indices is given in Appendix B.

For the Reno river, Tab. 5.2, the feature of the distributions are similar to the Panaro but more accentuated. For Secchia river, Tab. 5.3, the baseline, 1.5, and 3.0 degree scenarios become all platykurtic, meanwhile, the 2.0 degree scenario is near to be mesokurtic.

Table with statistic indexes relative to Reno PDF

Degree scenario	Mean	Median	STD	Skewness	Kurtosis	SNR
Baseline	12.65	0.0	21.59	1.83	2.69	0.58
1.5	31.02	22.69	34.79	2.36	5.19	0.89
2	50.69	39.65	42.44	0.83	-0.56	1.19
3	71.42	62.21	69.07	0.37	1.75	1.03

Table 5.2: Statistic indices relative to the PDF of the Reno river 5.33. The explicit form of indices is given in Appendix B.

Table with statistic indexes relative to Secchia PDF

Degree scenario	Mean	Median	STD	Skewness	Kurtosis	SNR
Baseline	1.39	0	2.01	0.99	-0.68	0.69
1.5	3.58	1.17	4.39	1.22	0.51	0.81
2	7.72	6.51	6.06	0.19	-1.42	1.27
3	11.74	10.83	7.40	0.40	-0.78	1.58

Table 5.3: Statistic indices relative to the PDF of the Secchia river 5.34. The explicit form of indices is given in Appendix B.

The last index computed is the Signal To Noise Ratio (SNR), as proposed by [30] (Qingyun Duan et al.). The simple model averaging (SMA) defined the signal as the arithmetic multimodel ensemble mean, and the noise as the intraensemble range, i.e. standard deviation. By definition when the SNR increases there is more agreement between models, and vice-versa when SNR decreases there is disagreement. Since there is no established threshold value for SNR, to make some statement about the quality of the signal subjective considerations can be done. When $SNR < 1$, the signal is smaller than the noise, we can assume that information contained in the mean is not very trustworthy. Instead, $SNR > 1$ could indicate that the values explored by the ensemble are close enough to consider the arithmetic multimodel ensemble mean as a representative signal. By referring to the values reported in the tables for all the rivers, the SNR value for baseline and 1.5-degree scenarios is smaller than 1, suggesting that any consideration performed by considering such signal could be misleading. However, by looking at 2.0 and 3.0-degree scenarios, SNR becomes greater than 1 by suggesting that the information contained in the signal is trustworthy, so a damage cost increasing, by increasing the temperature, would seem unavoidable. This result, the increasing of SNR with temperature increase, can be caused by the fact that the multi-model ensemble computes damages from projections that start from the early 2000s; but climate projections are affected by the so-called epistemic and stochastic uncertainty. While the second one is irreducible, the first one is reducible, because when a long period is considered, the fluctuations of each model compensate each other. So, for the baseline and 1.5-degree scenario, the years of projection taken into account are few, while for the 2.0 and 3.0-degree scenario the information seems to be more robust because the projections take into account more years.

In literature, it becomes a certainty that for every RCP scenario, which assumes an increasing greenhouse gas (GHG) emission, global warming is inevitable. This means that, on average, the temperature will increase leading to more moisture available for atmosphere events, like precipitation one. Since extreme precipitation events have a strong dependence on moisture content, we are expecting that extreme precipitation will increase faster than the mean events [31](Myles R. Allen et al.). Because flooding events depend on extreme precipitation events, rather than mean ones, we are expect-

ing an increase in the frequency and magnitude of flooding events, so an increase in river flood hazard. As indicated by [7](Dankers et al.)), for A2 and B2 GHG forcing scenario, the average annual precipitation for north Italy will decrease, meanwhile the annual maximum 5-day accumulated rainfall, which could be considered as an extreme precipitation indicator, will increase. These extreme events will lead to an increase in the discharge value of 100-year return period events in all seasons except summer [7]. Most important is the fact that, in European rivers like the Po and its tributaries, the 100-year return period events decrease about to 50 and sometimes 20 years, meaning that the probability associated with 100-year return period events will become twice or greater [7], [10](Alfieri et al.).

Following [12](Alfieri et al.), the increase of damage computed with a 4 degrees global warming level, due to RCP 8.5, compared to the one simulated in the baseline period could be, on average, about 500%. In our case, the increase of damage, computed by the model with a 3 degrees global warming level due to the same RCP, compared to our baseline is, on average, about 580%, 460% and 713% respectively for Panaro, Reno and Secchia river with a 3 degrees global warming level.

All these results cited, some more than others, allow us to corroborate our one: climate change will cause an increase in damage cost due to flooding risk increase for rivers located in North Italy.

Chapter 6

Summary and conclusions

In Chapter 2, by following the reports of the Intergovernmental Panel for Climate Change we have reviewed the concepts of risk, Disaster Risk Reduction and Climate Change Adaptation. Then the My Climate Risk lighthouse defined by World Climate Research Program (WRCP) is highlighted, as how the "top-down" and "bottom-up" approaches can work in this direction. In Chapter 3, the rationale of the model and how it was formulated is presented, with a focus on the hypothesis concerning the assumption that the statistic of flood height is ascribable to the river discharge. The datasets used, and how it's component interface are summarized, and then the modelling approach is shown. Chapter 4 concerns the outline followed by the model and functions implemented to compute flood damage function and the damage at certain GWLs. In Chapter 5, the model was initially subjected to a sensitivity test concerning the assumption of Area of Influence followed. Model validation is performed by comparing the river discharges and damages estimation in present climate with the observed ones. Finally, some properties of the multi-models ensemble are analysed. Then the last part concern the results, which are the estimate of the damage at certain GWLs, in form of box plots and Probability Density Function. Finally, through an analysis of the statistics indices, are made some considerations of climate signals in terms of damage.

In order to address the low confidence concerning precipitation and floods projection for future scenarios on a global scale, this model tries to make a quantitative estimate of the uncertainty by following the approach proposed by My Climate Risk. By dealing with the problem from a local point o view, it enables a bottom-up approach to climate risk by providing flexible tools which, by using open-source data from climate services, allow us to assess the risk in future climate scenarios. Another aim is the quantitative estimate of some possible adaptation measure which acts on hazard, exposure and vulnerability in order to find which of such measure lead to more efficient adaptation. The uncertainty which emerges from the future degree scenarios is composed of two components, an epistemic and stochastic one. The epistemic uncertainty derives from our state of knowledge of the atmosphere and its interaction with the other components of the earth system. By introducing the description of the unknown phenomena and improving the ones that we already know, we will be able to reduce that source of uncertainty. The stochastic uncertainty is due to the intrinsic nature of the atmosphere which is chaotic, this must lead us to accept that we will always be dealing with a source of uncertainty that can never be under our control, leading it to be irreducible, and leaving us only with the possibility of better quantifying it. A common way employed to split the two sources of uncertainty is to make an ensemble of different realizations obtained from a single model by performing projections that starts from different initial conditions to take into account the fact that also the state from which the projections start is not knowing with arbitrarily large accuracy. Concerning the uncertainty deducible by our

results, the ensemble is not composed by different running of the same model but from sixteen projections performed by fifteen models, in which for only one model we have two different realizations. As consequence, the uncertainty is quantifiable as a whole and splitting the two components is not possible. Therefore the uncertainty to which we refer for the model takes into account both components. Concerning the error that we make by following our assumption of Areas of Influence it is two orders of magnitude smaller than the ensemble uncertainty for all the rivers, both in present climate and at a GWL of 1.5 . For what concerns the river discharge validation, the relative errors (Appendix B) that we make by considering the simulated slope of the flood-frequency relationship are 30% for the Panaro river, 15% for the Secchia river, 50% (according to AdB) and 32% (according to Comune di Marzabotto) for Reno-Casalecchio, 41% (according to AdB) and 28% (according to Comune di Marzabotto) for Reno-Marzabotto. This is anyway affected by large intrinsic variability in the observations that could be quantified in future studies and may allow more quantitative statements on the validation of the model. Therefore the hypothesis of AoI is a weak source of uncertainty, this gives us confidence about its applicability. Although the river discharge validation for the Reno river is inconclusive, due to a lack of well-document and high-quality data, the results of the test concerning the Panaro and Secchia rivers indicate a small source of error in this approximation. As regards the climate signal, it emerges as the temperature of future degree scenarios increases (see 5.2), and a similar trend is reported by [3] for the precipitation signal. Therefore an increase in damage due to flooding events as the temperature increase is found, which is in agreement with the results of [7](Dankers et al.) and [10](Alfieri et al.). The AoI definition followed, allow the model to perform analysis for catchment which have similar geometry, e.g. the slope. Therefore, to enable it to work with others rivers, different formulations of AoI must be taken into account, according to the type of catchment considered. This is necessary because the soundness of the assumption, on which the model is based ($p(h_i)dp = g(Q(r_i))dQ$), depends on how the AoIs are chosen, i.e. which river point r_i is linked to the domain point i, interested by a flood event. The approach followed by the model can be implemented for other extreme events models, e.g. by founding the way through which to link the statistics of a variable, which drives the hazard, with another one given by climate projections, to make a forecast of the first one. In that way, a projection of the economic impact of such extreme events can be performed. Therefore, if achievable, in order to implement adaptation measures, useful tools would be provided to the policymakers on the local scale to deal with an increase in risk due to extreme events.

Appendix A

Concerning the outline represented in Fig. 4.1, in that appendix the rule of the functions will be explained. To run the model, the first python script which is executed is **Risk - init - base** which import from the **Risk - dict** the following variables, dictionaries, array etc... :

- **Damages**
  - is a dictionary which associate to each asset category the damage fraction value
- **Files**
  - is a dictionary which associate to each model a nc data file
- **MaxDamages**
  - is a dictionary which associate to each asset category a number, provided by engineering studies, it is the max damages that an asset can suffer
- **Hdamages**
  - is a one dimensional array containing the number $0, 0.5, 1, 1.5, 2, 3, 4, 5, 6$, which represent a flooding heights
- **FILE LU**
  - file containing information about the portion of surface covered by land

From **Risk - Function** the following function are imported:

- **make LUs**
  - take as input the file FILE-LU to convert him into a npy format
- **make H**
  - convert the flooding height maps for the return periods equal to 10, 20, 50, 100, 200, 500 years into npy format
- **make Hfit**
  - by using the six flooding height maps relative to each return period, an interpolation is performed in order to obtain the value of the coefficients that allow to the computation of the flooding height maps for a generic return period. The two coefficients are named Hfit0 and Hfit1
- **make - idxMAP river**

  - take as input the river networks and flooding heights map to perform a map labelled by three indices. The first two indices are the coordinate of the grid point in the flooding height map (finer grid, 100m) and the third contain the coordinate of the nearest point of the river network map (coarse grid, 5 km)

- **make - idxLUMAP**
  - perform the same things of the previous one, but considering a map of asset categories rather than river network

- **make - rm - LU**
  - take as input idxLUMAP and provide as output a map of land use with the same grid of flooding height map

- **make - damage - fast**
  - is a function which provides the damage in a domain point subject to a flood event. Is a function of land use (asset category), flooding height and max damage

- **read - model**
  - for each model of the ensemble, it reads the value of a river discharge simulated for a given return period

- **make - RPs**
  - for each model of the ensemble, in order to compute the river discharge value for a generic return period a linear fit is performed

- **make - baseline - damage**
  - which in turn import from **Risk - Function** the following functions: make - damage - fast, read - model, make - RPs, Hfit0, Hfit1, make - rm - LU and idxMAP. A one-dimensional return period array is defined, containing numbers which come from 49.88 to 3000, with 90 equidistant steps in a logarithmic space in order to explore several orders of magnitude. For each element of the array, which is a return period, the damage associated with such a return period is computed. A masked is applied in order to compute the damage only in the domain points which belong to an asset category defined before. Another mask is applied to consider only the point in which the Hfit0 and Hfit1 are different from zero, i.e. a domain point susceptible to a flooding event.

The last function analyzed is **make - GWL**. The procedure following this function is similar to **make - baseline - damage**. The input is the same as the previous function, a damage is computed in the present climate in the same way of make baseline damage, but by taking into account the ensemble of the models. The return period array considered now depends on the GCMs which is taken into account. The return periods explored, to compute the damage, depend on the GWL chosen and once again from GCM.

Appendix B

Concerning the relative errors in 5.1.4 and 6 are respectively computed as:

$$\frac{EFAS\ based - CMIP\ based}{EFAS\ based} \tag{6.1}$$

and

$$\frac{observed - CMIP\ based}{observed} \tag{6.2}$$

Concerning the Tab. 5.1, 5.2 and 5.3 in that appendix explicit forms of the indices reported are reported.

- **Mean** The mean value of expected damages the ensemble it is computed as the sum of all the expected damages x_i simulated by the multi-model ensemble divided by the number of members of the ensemble

$$\mu = \frac{1}{M}\sum_{i=1}^{M} x_i. \tag{6.3}$$

- **Median** The median value of expected damages is computed by sorting the expected damage computed by the member of multi-model ensemble and then computing the mean value between the values which occupies the positions $\frac{n}{2}$ and $\frac{n}{2}+1$

- **Standard deviation (STD)**

$$\sigma = \sqrt{\frac{1}{M}\sum_{i=1}^{M}(x_i - \mu)^2.}, \tag{6.4}$$

  where μ is the mean value of expected damages

- **Skewness** The sample skewness is computed as the Fisher-Pearson coefficient of skewness [32], i.e.

$$g_1 = \frac{m_3}{m_2^{3/2}}, \tag{6.5}$$

  where

$$m_i = \frac{1}{N}\sum_{i=1}^{N}(x[n] - \mu)^i, \tag{6.6}$$

  is the biased sample i-th central moment.

- **Kurtosis** The Kurtosis considered here is the Fisher one, computed as fourth central moment divided by the square of the variance minus 3 [32]

$$kurtosis = \frac{m_4}{\sigma^4} - 3, \tag{6.7}$$

- **Signal to Noise ratio (SNR)** The signal to noise ratio (SNR) is defined as the ratio between the mean and the STD

$$SNR = \frac{\mu}{\sigma}. \tag{6.8}$$

Bibliography

[1] P. Ruggieri et al. In: (2022).

[2] R. Shukla et al. "Climate Change and Land: an IPCC special report on climate change, desertification, land degradation, sustainable land management, food security, and greenhouse gas fluxes in terrestrial ecosystems". In: *IPCC* (2019).

[3] S.I. et al. Seneviratne. "The Physical Science Basis. Contribution of Working Group I to the Sixth Assessment Report of the Intergovernmental Panel on Climate Change ". In: *IPCC* (2021), pp. 1513–1766. DOI: 10.1017/9781009157896.013. URL: https://www.ipcc.ch/report/ar6/wg1/chapter/chapter-11/.

[4] et al. Lee J.-Y. "Future Global Climate: Scenario-Based Projections and Near-Term Information. In Climate Change 2021: The Physical Science Basis. Contribution of Working Group I to the Sixth Assessment Report of the Intergovernmental Panel on Climate Change". In: *IPCC* (2021), pp. 553–672. DOI: 10.1017/9781009157896.006. URL: https://www.ipcc.ch/report/ar6/wg1/chapter/chapter-4/.

[5] Regina R Rodrigues and Theodore G Shepherd. "Small is beautiful: climate-change science as if people mattered". In: *PNAS Nexus* 1.1 (Mar. 2022). ISSN: 2752-6542. DOI: 10.1093/pnasnexus/pgac009. URL: https://doi.org/10.1093/pnasnexus/pgac009.

[6] World Climate Research Programme. *Report on the WCRP My Climate Risk First General Assembly*. URL: https://www.wcrp-climate.org/my-climate-risk.

[7] Rutger Dankers and Luc Feyen. "Climate change impact on flood hazard in Europe: An assessment based on high-resolution climate simulations". In: *Journal of Geophysical Research: Atmospheres* 113.D19 (2008). DOI: https://doi.org/10.1029/2007JD009719. eprint: https://agupubs.onlinelibrary.wiley.com/doi/pdf/10.1029/2007JD009719. URL: https://agupubs.onlinelibrary.wiley.com/doi/abs/10.1029/2007JD009719.

[8] A. Libertino, D. Ganora, and P. Claps. "Evidence for Increasing Rainfall Extremes Remains Elusive at Large Spatial Scales: The Case of Italy". In: *Geophysical Research Letters* 46.13 (2019), pp. 7437–7446. DOI: https://doi.org/10.1029/2019GL083371. URL: https://agupubs.onlinelibrary.wiley.com/doi/abs/10.1029/2019GL083371.

[9] Lorenzo Alfieri et al. "Advances in pan-European flood hazard mapping". In: *Hydrological Processes* 28.13 (2014), pp. 4067–4077. DOI: https://doi.org/10.1002/hyp.9947. URL: https://onlinelibrary.wiley.com/doi/abs/10.1002/hyp.9947.

[10] L. Alfieri et al. "Global warming increases the frequency of river floods in Europe". In: *Hydrology and Earth System Sciences* 19.5 (2015), pp. 2247–2260. DOI: 10.5194/hess-19-2247-2015. URL: https://hess.copernicus.org/articles/19/2247/2015/.

[11] Lorenzo Alfieri et al. "Ensemble flood risk assessment in Europe under high end climate scenarios". In: *Global Environmental Change* 35 (2015), pp. 199–212. DOI: https://doi.org/10.1016/j.gloenvcha.2015.09.004. URL: https://www.sciencedirect.com/science/article/pii/S0959378015300406.

[12] Lorenzo Alfieri et al. "Global projections of river flood risk in a warmer world". In: *Earth's Future* 5.2 (2017), pp. 171–182. DOI: https://doi.org/10.1002/2016EF000485. URL: https://agupubs.onlinelibrary.wiley.com/doi/abs/10.1002/2016EF000485.

[13] Claussen et al. "Earth system models of intermediate complexity: closing the gap in the spectrum of climate system models". In: *Climate Dynamics* 18 (2002), pp. 579–586. DOI: https://doi.org/10.1007/s00382-001-0200-1.

[14] "Climate Change 2014: Impacts, Adaptation, and Vulnerability - AR5-WG2". In: *IPCC* (2014).

[15] "Climate Change 2013: The physical basis - AR5-WG1". In: *IPCC* (2013).

[16] Maria Carmen Llasat et al. "Trends in flash flood events versus convective precipitation in the Mediterranean region: The case of Catalonia". In: *Journal of Hydrology* 541 (2016). Flash floods, hydro-geomorphic response and risk management, pp. 24–37. ISSN: 0022-1694. DOI: https://doi.org/10.1016/j.jhydrol.2016.05.040. URL: https://www.sciencedirect.com/science/article/pii/S0022169416303079.

[17] E. J. Gumbel. "The Return Period of Flood Flows". In: *The Annals of Mathematical Statistics* 12.2 (1941), pp. 163–190. DOI: 10.1214/aoms/1177731747. URL: https://doi.org/10.1214/aoms/1177731747.

[18] Dottori et al. "River flood hazard maps for Europe and the Mediterranean Basin region. European Commission". In: *Joint Research Centre (JRC)* (2021). DOI: 10.2905/1D128B6C-A4EE-4858-9E34-6210707F3C81. URL: https://data.jrc.ec.europa.eu/dataset/1d128b6c-a4ee-4858-9e34-6210707f3c81.

[19] György Büttner et al. "Copernicus land monitoring service-corine land cover. user manual. Technical report". In: *Copernicus Publications* (2021).

[20] H. Huizinga et al. "Global flood depth-damage functions—methodology and the database with guidelines". In: *European commission* (2017).

[21] P. Scussolini et al. "FLOPROS: an evolving global database of flood protection standards". In: *Natural Hazards and Earth System Sciences* 16.5 (2016), pp. 1049–1061. DOI: 10.5194/nhess-16-1049-2016. URL: https://nhess.copernicus.org/articles/16/1049/2016/.

[22] P et al. Berg. "Hydrology related climate impact indicators from 1970 to 2100 derived from bias adjusted European climate projections". In: *Copernicus Data Store of the Climate* (2021). DOI: 10.24381/cds.73237ad6. URL: https://cds.climate.copernicus.eu/cdsapp#!/dataset/sis-hydrology-variables-derived-projections?tab=overview.

[23] V. et al. tegeka. "EFAS-Meteo: A European daily high-resolution gridded meteorological data set for 1990 – 2011". In: *JRC Tech. Report* (2013). DOI: 10.2788/51262.

[24] Agenzia Interregionale per il fiume Po.

[25] Agenzia Interregionale per il fiume Po. *Relazione idrologica idraulica*. URL: https://www.agenziapo.it/sites/default/files/allegati/E2.01.09_0690-04-01-013R-01_Relazione%20idrologica-idraulica_allegato.pdf.

[26] Autoridà di Bacino Reno - PSAI Reno - Titolo II. *Rischio Idraulico e Assetto della Rete Idrografica*. URL: https://ambiente.regione.emilia-romagna.it/it/suolo-bacino/sezioni/pianificazione/autorita-bacino-reno/psai/tavole-tit-ii-reno/reno-tavole.

[27] Comune di Marzabotto. *Relazione idraulica inerente il programma di riqualificazione urbana della stazione ferroviaria di Marzabotto*. URL: https://www.comune.marzabotto.bo.it/upload/marzabotto/gestionedocumentale/08.RI-Rel-idraulica_784_4316.pdf.

[28] Heinz Dieter Fill and Alexandre Arns Steiner. "Estimating Instantaneous Peak Flow from Mean Daily Flow Data". In: *Journal of Hydrologic Engineering* 8.6 (2003), pp. 365–369. DOI: 10.1061/(ASCE)1084-0699(2003)8:6(365). eprint: https://ascelibrary.org/doi/pdf/10.1061/%28ASCE%291084-0699%282003%298%3A6%28365%29. URL: https://ascelibrary.org/doi/abs/10.1061/%28ASCE%291084-0699%282003%298%3A6%28365%29.

[29] David M. Allen. "The Relationship Between Variable Selection and Data Agumentation and a Method for Prediction". In: *Technometrics* 16.1 (1974), pp. 125–127. DOI: 10.1080/00401706.1974.10489157. URL: https://www.tandfonline.com/doi/abs/10.1080/00401706.1974.10489157.

[30] Qingyun Duan and Thomas J. Phillips. "Bayesian estimation of local signal and noise in multimodel simulations of climate change". In: *Journal of Geophysical Research: Atmospheres* 115.D18123 (2010). DOI: https://doi.org/10.1029/2009JD013654.

[31] Myles R. Allen and William J. Ingram. "Constraints on future changes in climate and the hydrologic cycle". In: *Nature* 419 (2002), pp. 224–232. DOI: https://doi.org/10.1038/nature01092.

[32] "CRC Standard Probability and Statistics Tables and Formulae". In: *Chapman Hal* (2000), Section 2.2.24.1.